

Discovery of D25, a Potent and Selective MNK Inhibitor for Sepsis-Associated Acute Spleen Injury

Qiang Li, Linmao Ke, Dandan Yu, Han Xu, Zixuan Zhang, Rilei Yu, Tao Jiang, Yue-Wei Guo,* Mingzhi Su,* and Xin Jin*

Cite This: <https://doi.org/10.1021/acs.jmedchem.3c02441>

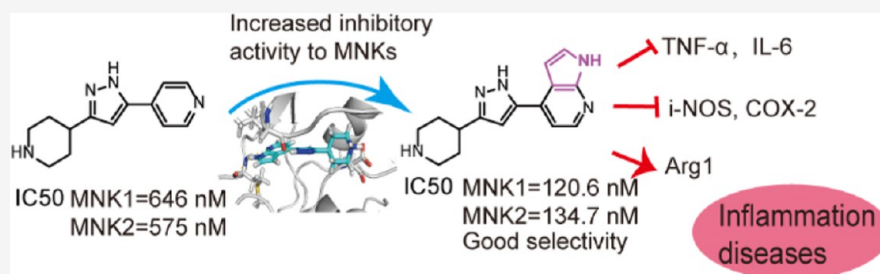
Read Online

ACCESS |

Metrics & More

Article Recommendations

Supporting Information



ABSTRACT: Mitogen-activated protein kinase-interacting protein kinases (MNKs) and phosphorylate eukaryotic initiation factor 4E (p-eIF4E) play a critical role in regulating mRNA translation and protein synthesis associated with the development of cancer, metabolism, and inflammation. This study undertakes the modification of a 4-(3-(piperidin-4-yl)-1H-pyrazol-5-yl)pyridine structure, leading to the discovery of 4-(3-(piperidin-4-yl)-1H-pyrazol-5-yl)-1H-pyrrolo[2,3-b]pyridine (D25) as a potent and selective MNK inhibitor. D25 demonstrated inhibitory activity, with IC₅₀ values of 120.6 nM for MNK1 and 134.7 nM for MNK2, showing exceptional selectivity. D25 inhibited the expression of pro-inflammation cytokines in RAW264.7 cells, such as inducible NO synthase, cyclooxygenase-2, and interleukin-6 (IL-6). In the lipopolysaccharide-induced sepsis mouse model, D25 significantly reduced p-eIF4E in spleen tissue and decreased the expression of tumor necrosis factor α , interleukin-1 β , and IL-6, and it also reduced the production of reactive oxygen species, resulting in improved organ injury caused by inflammation. This suggests that D25 may provide a potential treatment for sepsis and sepsis-associated acute spleen injury.

INTRODUCTION

Eukaryotic initiation factor 4E (eIF4E), a cap-dependent translation factor, plays an important role in the translation of mRNA that is involved in many biological processes,^{1,2} and its activity is regulated by the PI3K/Akt/mTORC1 and Ras/Raf/MAPK signaling pathways.³ The mitogen-activated protein kinase-interacting protein kinases (MNKs) comprise MNK1 and MNK2, which phosphorylate eIF4E at Ser209 in vitro and in vivo to regulate related protein synthesis and some biological processes.⁴ They are activated and regulated by Erk and, for MNK1, also by p38 MAP kinase. Overexpression of MNKs and eIF4E and elevated phosphorylation of eIF4E show a positive relationship with various cancers.⁵ MNKs can modulate the processes of cancer cell proliferation, migration, and metastasis by regulating the translation of specific mRNAs and thus the levels of the corresponding proteins, including cyclins, Snail, MMP-3,⁶ and Bcl-2.⁷ Phosphorylation of eIF4E is essential in tumorigenesis in some settings,⁸ but it is not necessary for normal conditions.^{9,10} MNKs may, therefore, be safe targets for the treatment of human diseases.

Sepsis, one of the most fatal diseases worldwide, often leads to multiple organ failure, mainly due to uncontrolled inflammatory responses.¹¹ The innate immune system is activated upon

infection by pathogenic microorganisms or tissue damage, which recruits macrophages to release inflammatory mediators such as tumor necrosis factor α (TNF- α), interleukin-6 (IL-6) and interleukin-1 β (IL-1 β), reactive oxygen species (ROS), nitric oxide (NO), prostaglandins, and inflammatory enzymes including inducible NO synthase (i-NOS) and cyclooxygenase-2 (COX-2), and all these mediators would arouse a cellular inflammatory response to pathogens or tissue damage.¹² Drug design for sepsis primarily targets pathogens (e.g., antibodies against lipopolysaccharide (LPS), TLR4 antagonists), inflammatory responses (e.g., anti-TNF α and IL-1 β antagonists), or coagulation cascades (e.g., platelet-activating factor inhibitors).¹³ However, the pathophysiological mechanisms associated with development and therapeutic targets of sepsis are largely unknown at present, and most drugs did not improve

Received: December 26, 2023

Revised: January 18, 2024

Accepted: January 24, 2024

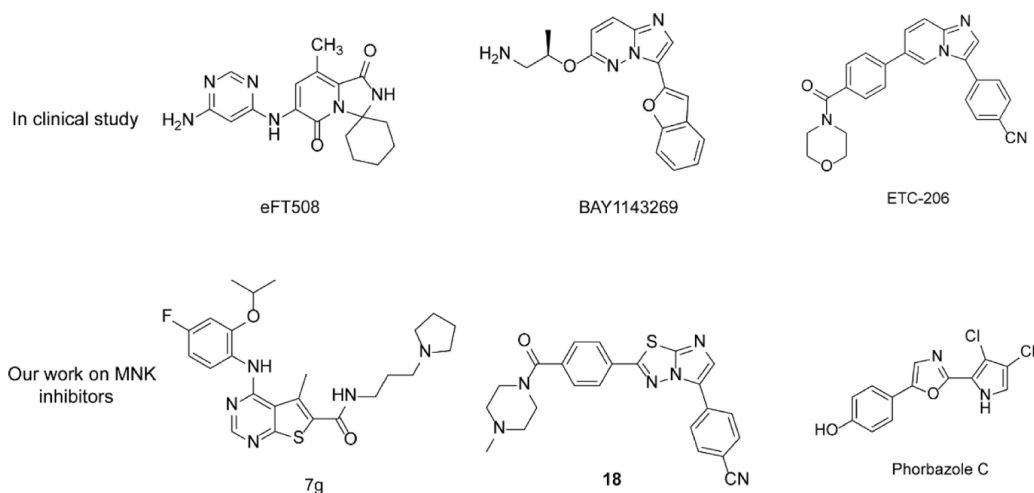
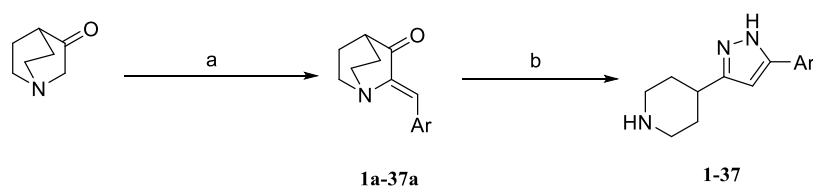


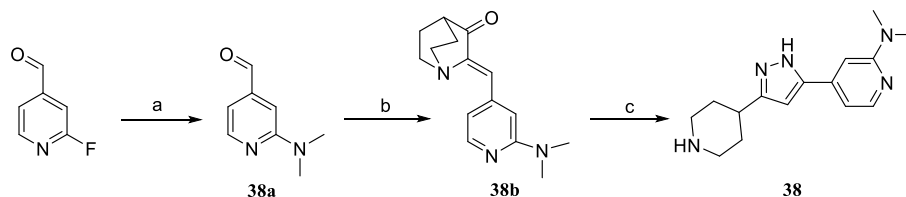
Figure 1. Chemical structures of MNK inhibitors that have been reported.

Scheme 1. General Synthetic Routes for Compounds 1–37^a



^aReagents and conditions: (a) NaOH, EtOH, Ar-CHO, 3 h; (b) 20% $\text{NH}_2\text{-NH}_2$, 2 h. For the structure of final compounds 1–37, see Tables 1–4.

Scheme 2. Synthetic Routes for Compound 38^a



^aReagents and conditions: (a) NaOH, DMF, 8 h; (b) 3-quinuclidinone hydrochloride, NaOH, EtOH, 3 h; (c) 20% $\text{NH}_2\text{-NH}_2$, 2 h.

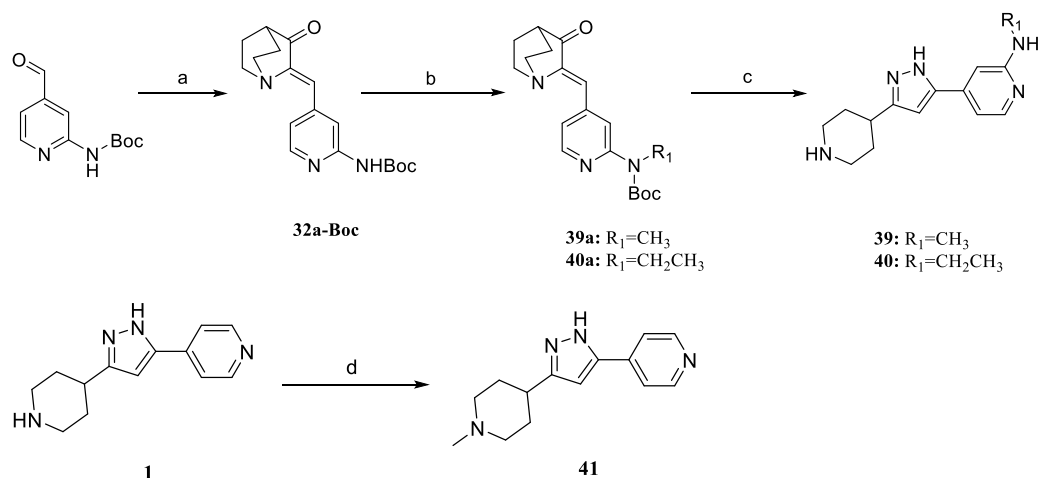
patient survival. Therefore, new candidate compounds or potential targets for sepsis are still needed.

The MAPK/MNK/eIF4E pathway is important for cytokine signaling and production.^{14–18} MNKs regulate multiple Toll-like receptor (TLR) signaling pathways, e.g. TLR2, TLR4, TLR6/2, and TLPR7¹⁹ and also modulate innate proinflammatory cytokine in macrophages (e.g., TNF- α , MCP-1, and IL-6).^{19,20} In a mouse model of LPS-induced acute lung injury, MNK2 knockout resulted in reduced lung histopathological changes, decreased neutrophil counts, and diminished production of IL-6, TNF- α , and keratinocyte-derived chemoattractants in mouse bronchoalveolar lavage fluid.²¹ In human keratinocytes, inhibition to MNK1 and the abolishment of eIF4E phosphorylation decrease the anisomycin-induced protein release of the pro-inflammatory cytokines TNF- α , IL-1 β , and IL-6.²² Furthermore, it has been proved that suppression of MNK2 in tumor-associated macrophages reprogrammed anti-inflammatory macrophages toward a proinflammatory phenotype with the ability to activate CD8⁺ T cells that can resist tumor development.²³ Altogether, pharmacological inhibitors of MNKs might have great potential in treating inflammatory

diseases in which bacterial products and innate, proinflammatory cytokines play a critical role in their pathogenesis.

Several MNK inhibitors have already been developed and studied as therapeutic agents for solid cancers, leukemia, and obesity, sometimes as a combination therapy with other agents.³ For several years, we have been developing MNK selective inhibitors,^{24–26} and most of them showed poor selectivity to MNKs (Figure 1). Currently three compounds (BAY1143269,²⁷ eFT508,²⁸ and ETC-206²⁹) have been studied in clinical trials for treating solid cancers and leukemia;³ their structures are shown in Figure 1. Of these compounds, only eFT508 is still in phase II (see clinicaltrials.gov).⁴ Currently, there are limited efficacy data and a scarcity of publications that support the use of small-molecule MNK inhibitors in treating inflammatory diseases.

Herein, we designed and synthesized series of novel MNK inhibitors with scaffolds of piperidine and pyrrole. Among these compounds, D25 showed potent activity against MNKs with IC_{50} of 120.6 and 134.7 nM, respectively, and good selectivity to MNKs against a panel of 70 kinases. We found that it exerted good anti-inflammation effects in macrophages in vitro and protected tissues from invasion of inflammatory cytokines

Scheme 3. Synthetic Routes for Compounds 39–41^a

^aReagents and conditions: (a) NaOH, EtOH, 3-quinuclidinone hydrochloride, 3 h; (b) NaH, CH₃I (39a) or CH₂CH₃I (40a), THF, 3 h; (c) 20% NH₂-NH₂, 2 h; DCM, CF₃COOH, NH₄OH; (d) formaldehyde, NaBH₄, CF₃COOH, THF, 2 h; NaOH, 24 h.

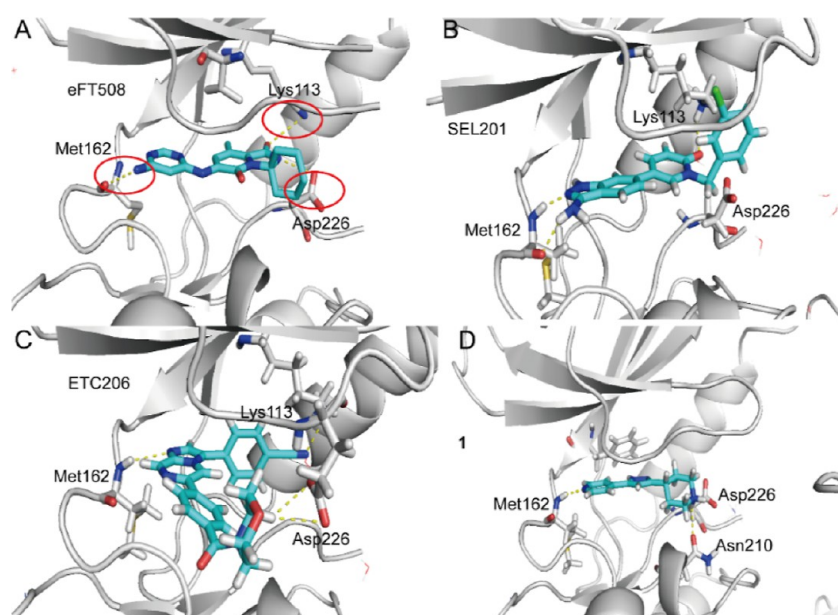


Figure 2. Binding mode of eFT508 (A), SEL201 (B), ETC206 (C), and compound 1 (D) to MNK2 (PDB:6ck6). Active site residues are shown as sticks; hydrogen bonds are indicated by dashed lines (yellow).

induced by LPS in vivo through regulating the axis of MNK/eIF4E and the releasing of TNF- α and IL-6.

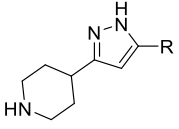
RESULTS AND DISCUSSION

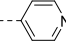
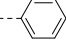
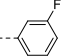
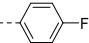
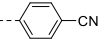
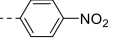
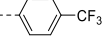
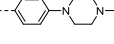
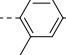
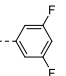
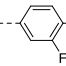
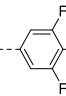
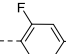
Chemistry. Compounds 1–37 were synthesized starting from material 3-quinuclidinone hydrochloride, which was converted into compounds 1a–37a with various substituted aromatic aldehydes in the presence of NaOH (sodium hydroxide) in ethanol.³⁰ Finally, 1a–37a were treated with hydrazine to give compounds 1–37 (Scheme 1). 2-Fluoroisoinicotinaldehyde can be transformed into 38a in the presence of NaOH and DMF (*N,N*-dimethylformamide) and then 38a reacted with 3-quinuclidinone hydrochloride and hydrazine to generate 38 (Scheme 2). 39a and 40a can be formed in the presence of 32a-boc, NaH (sodium hydride) and iodomethane or iodoethane, and then compounds 39–40 can be prepared by refluxing with excess of hydrazine hydrate (Scheme 3). *N*-

methylpiperidine 41 was made by a reductive amination of compound 1 with formaldehyde and sodium borohydride (Scheme 3).

Molecular Design Strategy to the Novel MNK Inhibitor Chemotype. MNKs belong to the family of Ca²⁺/calmodulin (CaM)-modulated protein kinases but differ from them.³¹ MNK1 and MNK2 possess a unique DFD (Asp-Phe-Asp) motif in the ATP binding pocket of their catalytic domains, which is strictly DFG (Asp-Phe-Gly) in other protein kinases.^{32,33} The special motif in the binding pocket makes it more difficult to get highly specific MNK inhibitors. Our approach to MNK inhibitor design focused on the interaction of hinge residues Leu127 in MNK1 and Met162 in MNK2 as well as the DFD motif domain. We conducted the analysis of the interaction maps, assessing the relationships between the specific and potent inhibitors (eFT508, SEL-201, and ETC-206) and the MNK2 protein complex (PDB:6ck6, Figure 2A–C). Together, we found some

Table 1. SAR of Compounds 1–13 and Their Physicochemical Properties



Compound	R	% inhibition at 5 μ M		Inhibition(%) at 20 μ M	Predicted LogP ^c	Predicted Caco-2 ^c
		MNK1 ^a	MNK2 ^a	MV-4-11 ^b		
1		84.99	90.44	51.2	1.395	-5.01
2		13.68	4.81	0.3	2.567	-4.988
3		14.14	7.05	0.1	2.714	-5.009
4		82.25	90.77	0.1	2.635	-5.001
5		-9.61	9.73	6.0	2.213	-5.007
6		3.24	-4.12	4.6	2.58	-5.013
7		19.27	-15.27	36	3.669	-5.046
8		2.31	6.42	8.5	2.331	-5.554
9		7.30	7.61	31.2	1.433	-5.344
10		8.83	3.46	2.1	2.858	-5.079
11		7.77	-12.06	6.4	2.889	-5.026
12		18.88	14.2	3.4	3.155	-5.187
13		3.12	-7.79	9.8	2.775	-5.009

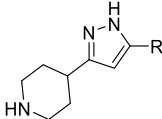
^aIn vitro inhibition to MNK1 and MNK2 at 5 μ M; average of two determinations. ^bCell proliferation inhibition measured using the MV-4-11 cell line, average of three determinations. ^cProperties of log *P* and Caco-2 were predicted using the online tool of ADMETlab 2.0 (<https://admetmesh.scbdd.com/>); optimal: 0–3 (for log *P*); > -5.15 (for caco-2).

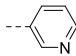
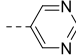
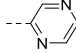
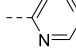
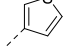
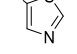
key interactions with the MNK2 protein in the binding pocket: (i) the hydrogen bond with Met162 in the hinge region, (ii) the hydrogen bond with Asp226 in the DFD domain, and (iii) the hydrogen bond with Lys113.

Armed with this information, we initially aimed to identify a novel core skeleton. Previously, Julen Oyarzabal and colleagues reported a number of fragments identified through virtual screening, which could be used in the design of MNK

inhibitors.³⁴ Among them, the structure of 4-(3-(piperidin-4-yl)-1*H*-pyrazol-5-yl)pyridine (hit compound, compound 1) demonstrated moderate inhibition of MNK1 and MNK2 with IC₅₀ values of 646 and 575 nM, respectively. In addition, it showed good selectivity against a panel of 24 protein kinases. We found this scaffold to be an attractive starting point for generating novel inhibitors of MNK1/2 with drug-like properties.

Table 2. SAR of Compounds 14–19 and Their Physicochemical Properties



Compound	R	% inhibition at 5 μ M		Inhibition(%) at 20 μ M	Predicted LogP ^c	Predicted Caco-2 ^c
		MNK1 ^a	MNK2 ^a	MV-4-11 ^b		
14		7.43	11.73	0.2	1.296	-5.004
15		35.75	3.15	0.1	0.704	-5.08
16		20.09	11.98	0.1	0.905	-4.989
17		69.85	75.17	0.2	0.821	-4.976
18		4.32	6.20	0.1	2.292	-5.059
19		11.32	16.89	11.1	1.483	-4.989

^aIn vitro inhibition to MNK1 and MNK2 at 5 μ M; average of two determinations. ^bCell proliferation inhibition measured using the MV-4-11 cell line, average of three determinations. ^cProperties of log *P* and Caco-2 were predicted using the online tool of ADMETlab 2.0 (<https://admetmesh.scbdd.com/>); optimal: 0–3 (for log *P*); > -5.15 (for caco-2).

Molecular modeling was utilized to understand how the hit compound (compound 1) interacts with MNK1/2 and to guide our efforts in optimizing its potency. As the ATP binding sites of MNK1 and MNK2 share high sequence homology, we used the software of a Molecular Operating Environment (MOE) to elucidate the interaction between the MNK2 protein (PDB:6ck6) and compound 1. Our results indicated that it shared a similar combination mode with the ligand (eFT508) (Figure 2D). Specifically, the nitrogen atom of pyridine formed a hydrogen bond with Met162 of the hinge region, and the piperidine ring formed two hydrogen bonds' interaction with Asp226 of the DFD domain and Asn210. Although docking studies elucidated the interaction mode between compound 1 and MNK2, the structure–activity relationship (SAR) of this compound has not been explored. Consequently, we proceeded to introduce different substituents to enhance the MNK inhibitory activity.

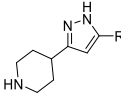
We made alterations to the pyridine structure, changing it to a benzene ring and/or incorporating one substituent to enhance bonding in the hydrophobic pocket (compounds 2–8, Table 1). We assessed their inhibitory activity against MNK1/2 at 5 μ M in vitro. The results revealed that only compound 4 (with 82.25% inhibition to MNK1 and 90.77% inhibition to MNK2) demonstrated inhibition to MNKs comparable to that of compound 1 (positive control, with 84.99% and 90.44% inhibition to MNK1/2, respectively). Other compounds did not exhibit obvious inhibitory activity to MNKs. We hypothesized that the fluorine atom on benzene might form a hydrogen bond with Met126 in the hinge region, thereby retaining MNK inhibition. Subsequently, we synthesized an

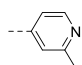
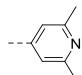
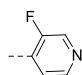
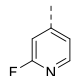
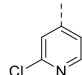
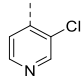
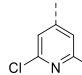
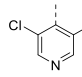
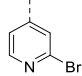
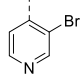
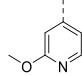
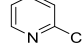
additional five compounds with 2–3 fluorine atoms or other groups at different positions on the benzene ring (compounds 9–13, Table 1). The results showed additional substitutions on benzene significantly decreased the MNK inhibitory activity.

We then shifted our focus onto the potential use of aromatic heterocycle compounds in this system. We introduced pyrimidine, pyrazine, thiophene, and thiazole into this class of structure (compounds 14–19, Table 2). The results showed all of these compounds either lost or showed decreased inhibitory activity against MNK1 and MNK2. When the R group was altered to 3-pyridine, 5-pyrimidine, 2-pyrazine, 3-thiophene, and 2-thiazole, compounds lost most of their MNK inhibitory activity. However, when the R group was 2-pyrimidine (compound 17), partial MNK inhibitory activity was retained, showing 69.85% inhibition to MNK1 and 75.17% inhibition to MNK2. These data suggested 4-pyridine was the optimal group for maintaining binding affinity and that the introduction of other heteroatoms would decrease the MNK inhibitory activity.

Based on this information, we introduced different substituents at the 4-pyridine group (compounds 20–31, Table 3). When substituents were introduced at the ortho-position of 4-pyridine, the inhibitory activity of MNKs of the compounds decreased significantly. When substituents were introduced at meta position of 4-pyridine, the inhibitory activity of MNKs was better than those with substituents at the ortho-position (for instance, compounds 22 and 25 showed better inhibition to MNKs than compounds 23 and 24). Moreover, when we introduced small substituents at the meta position of 4-pyridine, the inhibition to MNKs increased. Compound 22, with a F atom at the meta position of 4-pyridine, showed the best inhibitory

Table 3. SAR of Compounds 20–31 and Their Physicochemical Properties



Compound	R	% inhibition at 5 μ M		Inhibition (%) at 20 μ M	Predicted LogP ^c	Predicted Caco-2 ^c
		MNK1 ^a	MNK2 ^a	MV-4-11 ^b		
20		53.3	39.77	0.1	1.709	-4.972
21		22.53	-2.45	0.2	2.076	-5.205
22		92.14	92.54	0.1	1.422	-4.951
23		51.18	61.79	0.1	1.691	-4.928
24		18.87	10.10	35.6	2.158	-4.977
25		83.14	82.71	32.8	2.078	-4.95
26		45.63	12.52	22.1	3.254	-5.027
27		55.58	59.45	19.6	2.665	-5.001
28		12.01	2.35	20.7	2.398	-4.976
29		68.68	72.50	6.1	0.974	-5.18
30		30.09	13.50	19.3	1.996	-5.014
31		22.53	30.78	52.5	2.314	-4.98

^aIn vitro inhibition to MNK1 and MNK2 at 5 μ M; average of two determinations. ^bCell proliferation inhibition measured using the MV-4-11 cell line, average of three determinations. ^cProperties of log *P* and Caco-2 were predicted using the online tool of ADMETlab 2.0 (<https://admetmesh.scbdd.com/>); optimal: 0–3 (for log *P*); > -5.15 (for caco-2).

activity to MNKs, outperforming compounds **25** and **29**. We supposed that the substituents at the ortho position might affect the formation of the hydrogen bond between the nitrogen atom

of pyridine and Met162. On docking compounds **22** (Figure 3A,B) and **23** (Figure 3C,D) into the protein of MNK2 to access how the substituents affect the interaction with MNKs, we noted

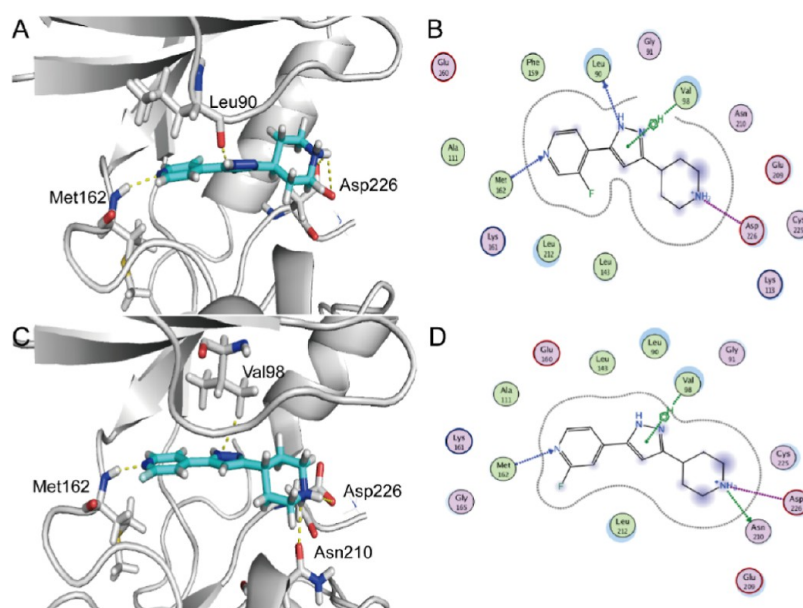


Figure 3. Docking mode of compounds **22** (A,B) and **23** (C,D) with MNK2 (PDB:6ck6). Active site residues are shown as sticks; hydrogen bonds are indicated by dashed lines (yellow in A,C).

from the docking map that substituents at the meta position of 4-pyridine face toward the center of the ATP binding pocket (Figure 3). When a large or bulky group is introduced at the ortho- or meta-position, it interferes with the binding affinity of the hydrogen bond between the nitrogen atom of pyridine and Met126 of the hinge region and between the NH of pyrazole and Leu90. This effect becomes more pronounced when the substituents are at the ortho-position due to their proximity to the residue Met162, which increases the distance between the nitrogen atom of pyridine and Met162, resulting in the interaction with Met162 and Leu90 fading away and the compounds losing the inhibition to MNKs.

Meanwhile, we observed that the oxygen atom of Met162 is close to the ortho-position of 4-pyridine. We hypothesized if we introduced a hydrogen bond donor group at this position, it could increase the binding affinity to MNKs. Therefore, we synthesized compound **32**, which harbors both a hydrogen bond donor and a hydrogen bond receptor. The inhibition to MNKs was increased when we introduced the $-\text{NH}_2$ group at the ortho-position of 4-pyridine as per our assumption. Compound **32** exhibited potent inhibition to MNK1 and MNK2 at $5 \mu\text{M}$ (89.5% inhibition to MNK1 and 96.18% inhibition to MNK2). Modeling of compound **32** into the ATP pocket of MNK2 helped us understand their interaction mode, and the result showed that the nitrogen atom of pyridine and $-\text{NH}_2$ formed two hydrogen bonds with Met126, very similar to the interaction established by the ligand of eFT508. This hydrogen bond is stable during the molecular dynamics (MD) simulations (Figure 4A). Enhancing binding affinity with MNK2 results in improved MNK inhibition. The results indicated that a hydrogen bond donor at the ortho-position of pyridine could enhance the interaction with MNKs. To confirm this conclusion, we designed and synthesized compounds **33–36**, each with a hydrogen bond donor and a hydrogen bond acceptor. Surprisingly, compounds **33–35** did not show good inhibition as compound **32** showed, which suggested that only the 4-pyridine group could bind with MNK active residues. Compound **36** showed the most potent inhibitory activity against MNK1 and MNK2 at $5 \mu\text{M}$ (98.68% inhibition to

MNK1; 97.44% inhibition to MNK2). In our docking model, compounds **34–36** all have the same interaction mode with protein as compound **32** and **36** showed, but the inhibition to MNKs was quite different. We proposed that the stability of the hydrogen bond might affect the results. Therefore, we ran MD simulations of the hydrogen bonds 1 (between the nitrogen atom of pyridine and Met126) and 2 (between the NH atom of pyridine and Met126) from compounds **33** and **36** (Figure 4B,C). All the compounds can form a stable hydrogen bond 1, but the hydrogen bond 2 from compound **33** is weak with a distance of 3.8 Å. Additionally, compound **33** also loses its interaction with the DFD area of the protein, which leads to a decrease in the inhibition to MNKs. All the results showed us that it was important for 4-pyridine to maintain all the key interactions with MNK proteins and introducing an $-\text{NH}$ group at the ortho-position of 4-pyridine would increase the inhibition to MNK1 and MNK2.

We also synthesized compounds **37–40** (Table 4) and found that compounds **37** and **38** lost most of the inhibitory activity to MNKs, which further supported the fact that the introduction of $-\text{NH}$ at the ortho-position of 4-pyridine would increase the binding affinity with MNKs. Compounds **39** and **40** keep partial inhibition to MNKs, which indicated that introducing substituents at $-\text{NH}_2$ of 4-pyridine would decrease the inhibitory activity against MNKs. When we introduced a $-\text{CH}_3$ at piperidine of compound **1** (compound **41**), inhibition to MNKs was decreased compared to compound **1**, confirming the importance of the $-\text{NH}$ of the piperidine ring in the interaction with MNKs. Taken together, we identified a potent and novel MNK inhibitor-compound **36** (named D25) with IC_{50} values of 120.6 and 134.7 nM for MNK1 and MNK2 assays, respectively (Table 5).

Kinase Selectivity. D25 was tested against a panel of 70 kinases. D25 at $1 \mu\text{M}$ inhibits only MNK1 and MNK2 at $>80\%$, with the inhibition of 88.34 and 85.85%, respectively, 5 kinases (IKK α , QIK, HGK, CHK2, AMPK α 1/ β 1/ γ 1) at 50–70%, which indicated that D25 has a good selectivity against these kinases (Figure 5 and Table S1).

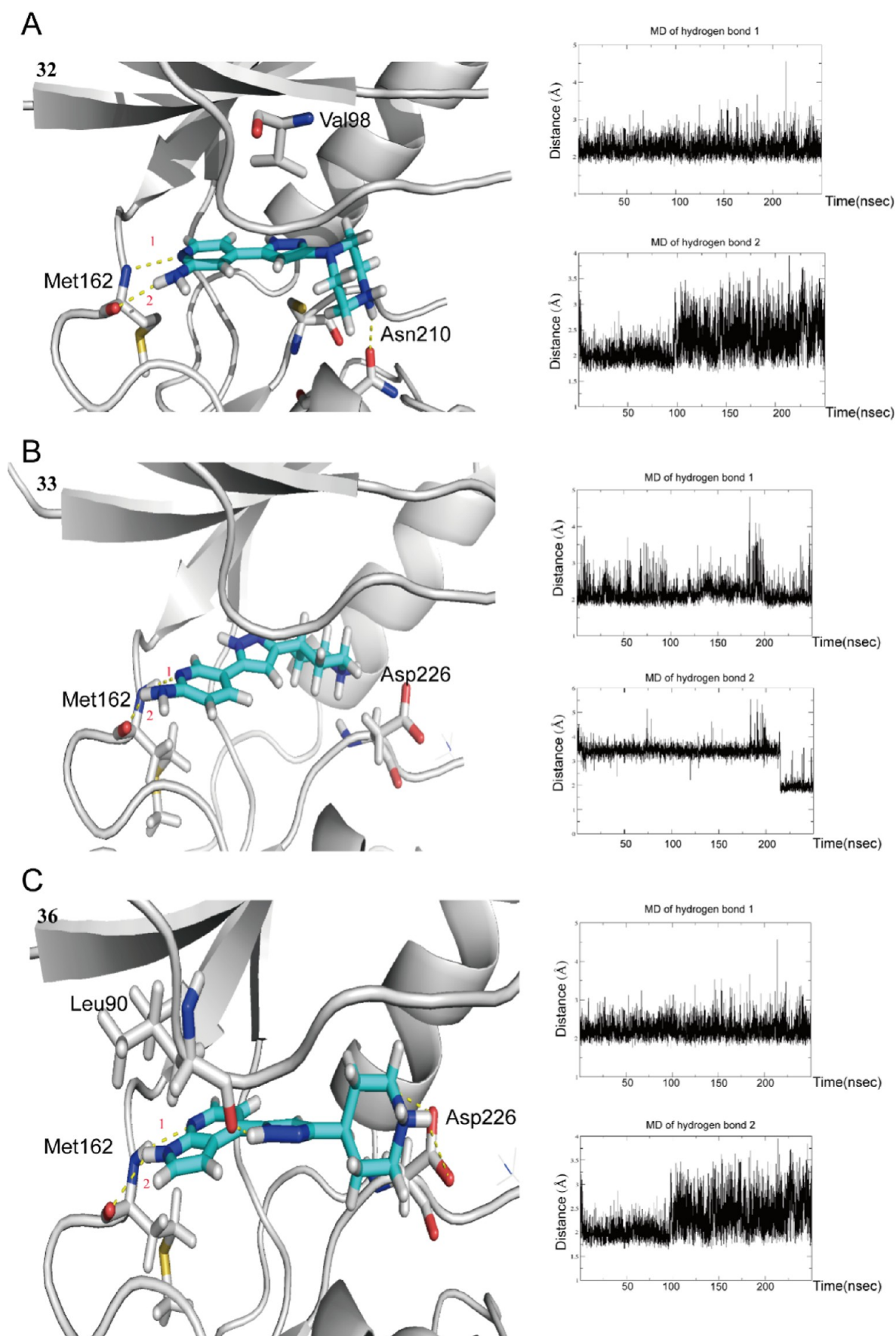
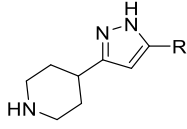
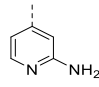
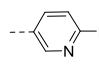
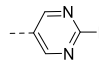
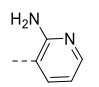
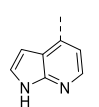
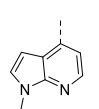
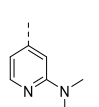
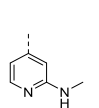
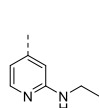


Figure 4. Docking mode of compounds 32 (A), 33 (B), and 36 (C) with MNK2 (PDB:6ck6) and the distance of the hydrogen bonds during the MD simulations. Active site residues are shown as sticks; hydrogen bonds are indicated by dashed lines (yellow).

Table 4. SAR of Compounds 32–41 and Their Physicochemical Properties



Compound	R	% inhibition at 5 μ M		Inhibition (%) at 20 μ M	Predicted LogP ^c	Predicted Caco-2 ^c
		MNK1 ^a	MNK2 ^a	MV-4-11 ^b		
32		89.50	96.18	33.3	1.027	-5.361
33		20.28	5.47	35.0	0.943	-5.43
34		22.08	-0.02	37.9	0.709	-5.473
35		41.07	34.55	15.2	1.083	-5.202
36		98.68	97.44	98.5	1.754	-5.196
37		12.32	17.37	23.8	1.984	-5.087
38		7.51	7.62	56.9	1.983	-4.906
39		62.68	80.17	30.2	1.612	-5.379
40		49.63	74.10	15.4	2.154	-5.278
41	---	79.71	87.34	3.39	1.918	-4.607

^aIn vitro inhibition to MNK1 and MNK2 at 5 μ M; average of two determinations. ^bCell proliferation inhibition measured using the MV-4–11 cell line, average of three determinations. ^cProperties of log *P* and Caco-2 were predicted using the online tool of ADMETlab 2.0 (<https://admetmesh.scbdd.com/>); optimal: 0–3 (for log *P*); > -5.15 (for caco-2).

Table 5. IC₅₀ Values of MNK1 and MNK2 Inhibitor Analogues 4, 22, 32, and 36

compound	IC ₅₀ (nM)	
	MNK1	MNK2
4	1800	586.7
22	595.9	574.5
32	401.4	198.8
36	120.6	134.7
STSP	48.96	11.02

Biological Activity Evaluation. Compound 1 has been reported to inhibit cell proliferation in MV-4–11 cells with an EC₅₀ of 17 μ M.³⁴ We also tested our compounds at 20 μ M on this cell line, and the result showed that most of the compounds did not inhibit the cell proliferation, except for compound 36. Its inhibition reached 98% at 20 μ M with an IC₅₀ of 0.55 μ M, which is superior to what was shown by the hit compound (1). Existing studies have disclosed that MNKs are not necessary for cell proliferation and development.⁸ However, certain pro-inflammatory cytokines and chemokines impact both tumor cell

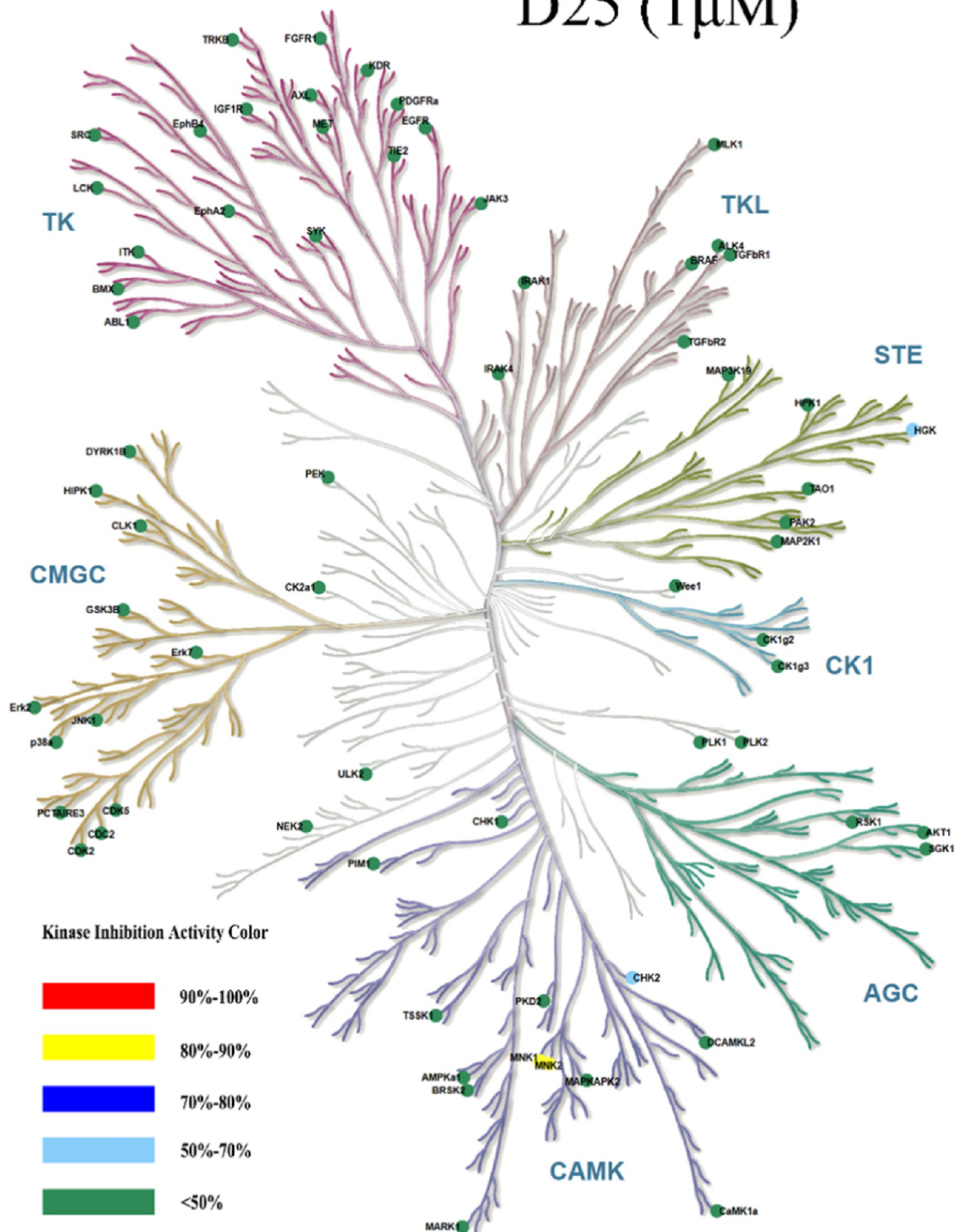
D25 (1 μ M)

Figure 5. Kinome plot depicting the selectivity of D25 across 70 kinases at 1 μ M.

survival signaling and the composition and signaling of the TME, which, in turn, affects cancer survival.^{7,28} eFT508 has

significant effects on multiple pro-tumorigenic cytokines (TNF- α , IL-6, and IL-8) and mediate tumor progression.²⁸ It is thus

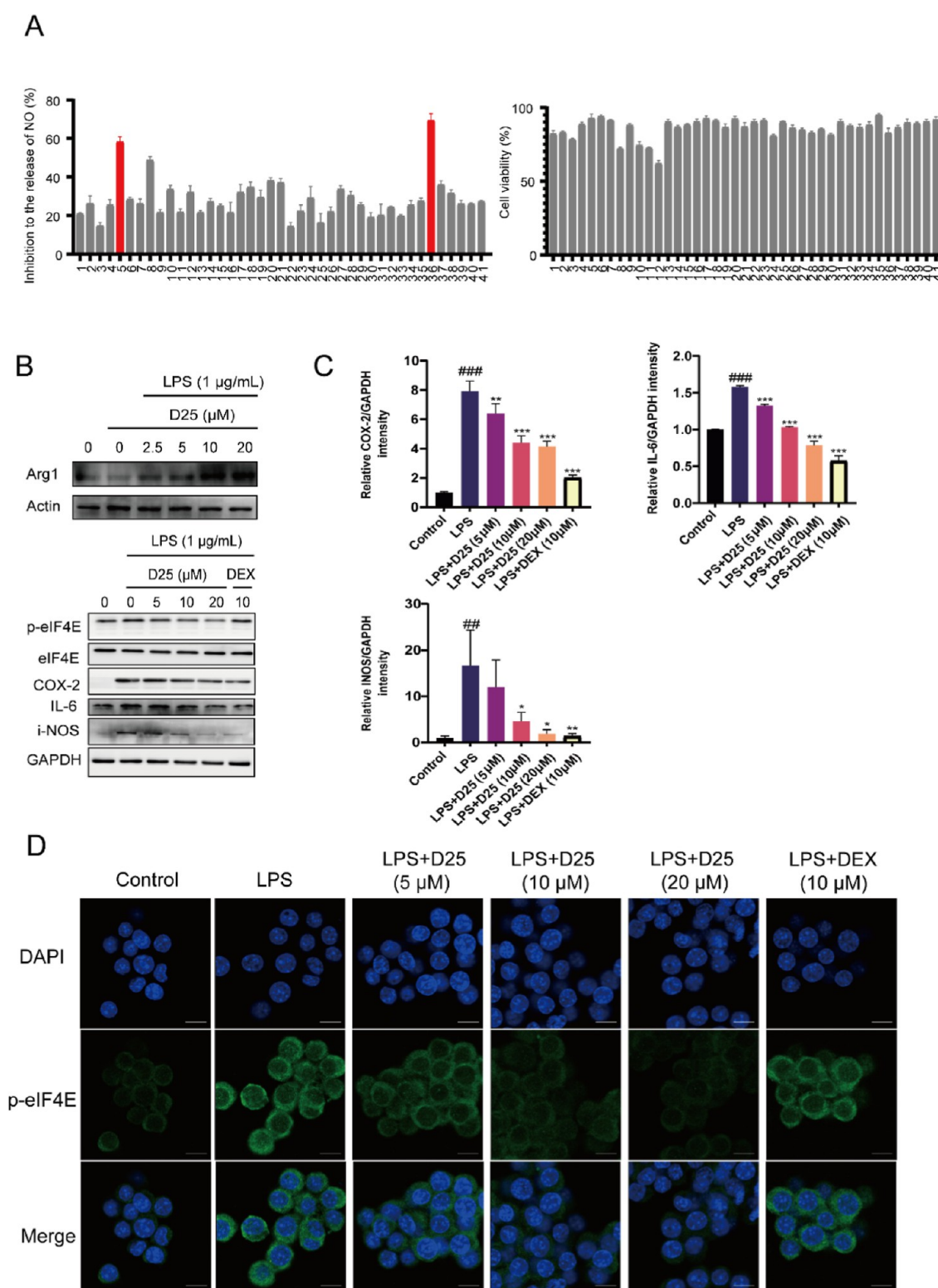


Figure 6. MNK inhibitor D25 exerted anti-inflammation effects in RAW264.7 cells. (A) Effects of compounds on the inhibition to the release of NO and cell viability, $n = 3$. (B) Western blot analysis of indicated protein expression in RAW264.7 cells with or without stimulation by LPS after the treatment of D25 at indicated concentrations; DEX serves as a positive control. (C) Quantification of data from three independent experiments for COX-2, IL-6, and i-NOS. (D) Representative images of nucleus marker (blue) and p-eIF4E marker (green), magnification: 200 \times , scale bar: 100 μm ; $##p < 0.01$, $###p < 0.001$ vs controls; $*p < 0.05$, $**p < 0.01$, and $***p < 0.001$ vs LPS-treated cells.

plausible that D25 may regulate some cytokines to affect the viability of MV-4–11 cells.

LPS triggers the release of inflammatory mediators from macrophages, including TNF- α , IL-1 β , and IL-6. We then tested

the effects of all the compounds on inflammation induced by LPS in Raw264.7 macrophages. The pro-inflammatory cytokines induced by LPS lead to increased expression of i-NOS and COX2 in endothelial cells and vascular smooth muscle

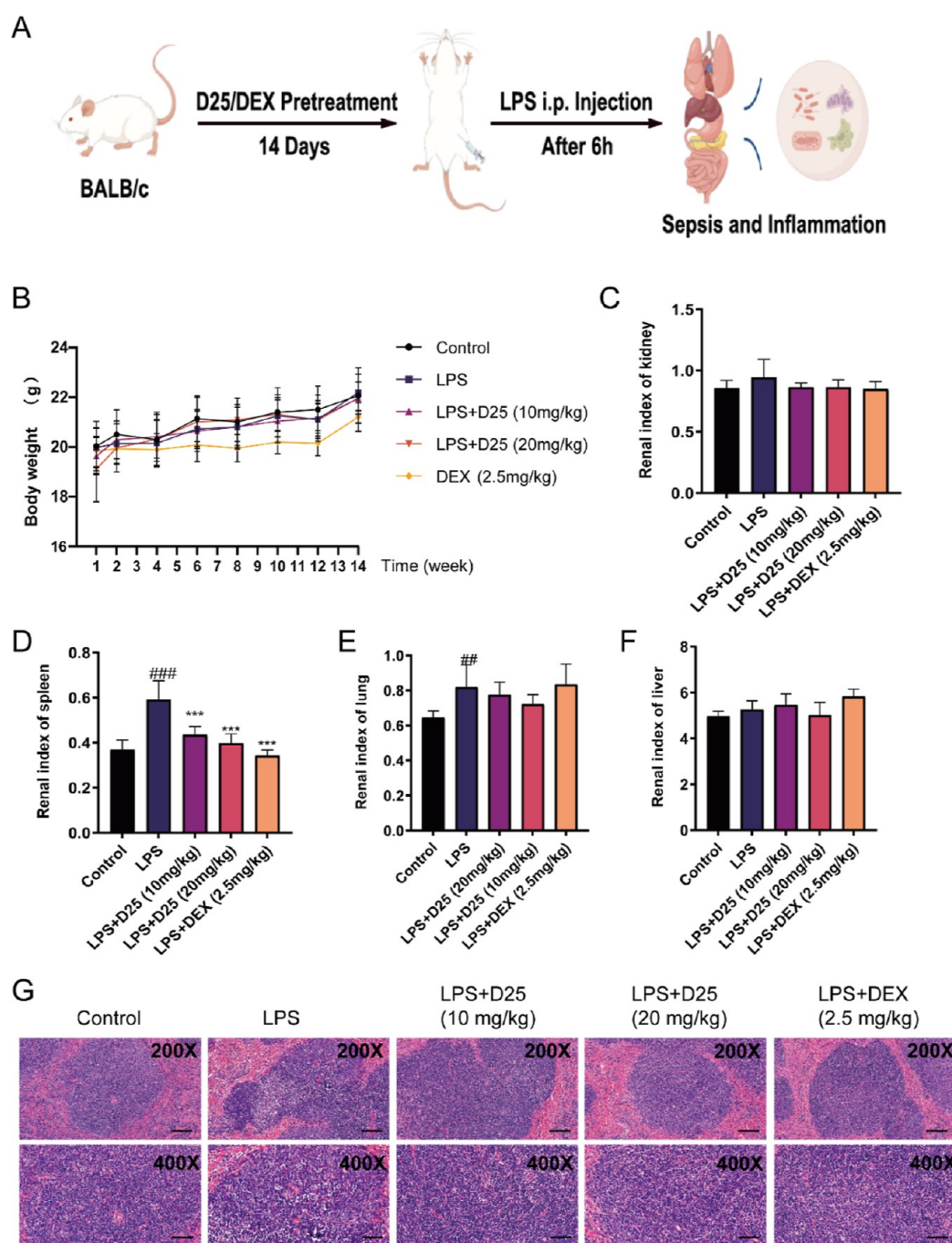


Figure 7. Effects of D25 on LPS-induced sepsis and dysfunction. (A) Brief flow diagram of the experiment. (B) Body weight of mice from each group in 14 days, $n = 8$. (C–F) Index of the kidney, spleen, lung, and liver of each group, $n = 8$. (G) Spleen tissue samples from each group were stained for H&E. Representative images of H&E staining are shown at 200 \times and 400 \times magnification showing spleen injury in the control group, LPS alone group, and LPS with D25 or DEX group at indicated concentrations, scale bar: 100 μm . ### $p < 0.01$, ### $p < 0.001$ vs controls; *** $p < 0.001$ vs LPS-treated cells.

cells, which increases the production of NO.¹³ We used the Griess reagent to test the concentration of NO induced by LPS to evaluate the anti-inflammatory effects of the compounds. Compound **5**, **8**, and **36** showed inhibition over 50%, and only compound **36** showed 70% inhibition at 20 μM with potent MNK inhibition activity at the same time (Figure 6A). Other MNK inhibitors (**1**, **22**, and **32**) showed weak inhibition to the release of NO without obvious toxicity in cell viability assays (Figure 6A). We also analyzed the related protein expression of Arg1, COX-2, IL-6, and i-NOS in Raw264.7 cells treated with D25 at different concentrations and DEX (dexamethasone, as

positive control) following LPS induction (Figure 6B). Arginase 1 (Arg1) is a molecule known to be important in macrophage-mediated protection against injury.³⁵ Also, we noticed that the expression of Arg1 decreased after LPS treatment, and D25 increased its expression in a concentration-dependent manner. D25 at 10 μM or a higher concentration decreased the expression of p-eIF4E (a substrate of MNKs) and pro-inflammatory cytokines i-NOS, IL-6, and COX-2 (Figure 6C). Consistent with the decreased expression of p-eIF4E we observed, LPS induced more eIF4E phosphorylation in the cytoplasm of RAW264.7 cells, and D25 inhibited the expression

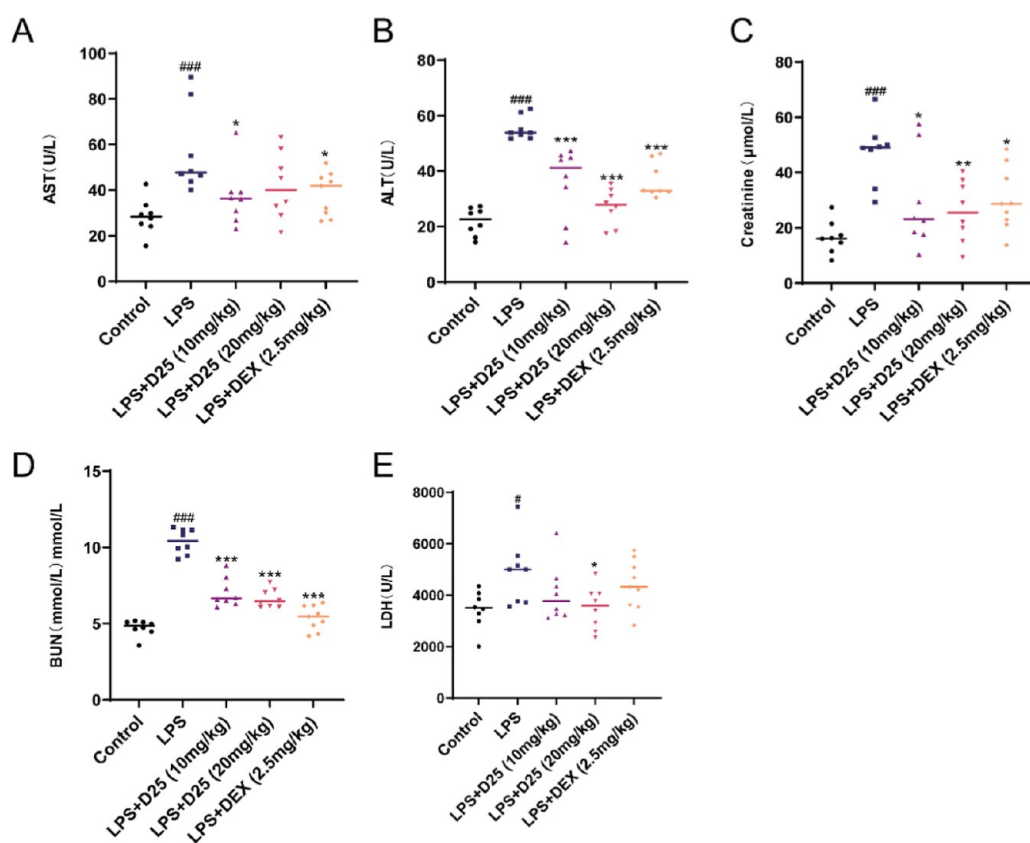


Figure 8. Effects of D25 on liver and kidney indicators. (A) Levels of AST in serum. (B) Levels of ALT in serum. (C) Levels of creatinine in serum. (D) Levels of BUN in serum. (E) Levels of LDH in serum; $n = 8$ mice per group. # $p < 0.05$, ### $p < 0.001$ vs controls. * $p < 0.05$, ** $p < 0.01$, and *** $p < 0.001$ vs LPS-treated cells.

of p-eIF4E by inhibiting the activity of MNKs in a concentration-dependent manner (Figure 6D). Taken together, our novel MNK inhibitor, D25, decreased the production of COX-2, IL-6, and i-NOS induced by LPS, suggesting its potential use as an anti-inflammatory agent.

Since D25 can inhibit the production of some anti-inflammatory factors and has a weak antitumor effect, we wondered whether it could act on inflammatory diseases. The LPS-induced sepsis mouse model is widely used for studies on pathogenesis and drug development.³⁶ We treated BALB/c mice with saline, D25 at the indicated concentration, and DEX (2.5 mg/kg) for 14 days (Figure 7A). There were no significant changes in the body weight of mice during the treatment with our compounds, indicating that D25 was an oral safe compound (Figure 7B). On the final day, LPS (10 mg/kg) was administered by intravenous injection. After 6 h, we examined the pathology all the tissues. The renal index of the kidney, spleen, liver, and lung showed that LPS had induced acute injury in the spleen and lung, especially in the spleen (Figure 7C–F). D25 at 20 mg/kg and DEX could reverse the situation significantly. To confirm the protective effect of D25 on the spleen, we performed a histopathological examination of the spleen in each group (Figure 7G). Spleen tissue sections from control mice showed a neat arrangement and structurally intact cells without deformation and necrosis. After LPS induced ASI (acute spleen injury), the sections showed a cell gap and the volume of the nucleus increased and increased inflammatory cells. However, after treatment with different concentrations of D25 and DEX, the abnormalities caused by LPS were effectively alleviated.

We measured the level of AST, ALT, BUN, LDH, and creatinine in serum, which are indicators of the liver and kidney. The abnormal increases of them showed impaired tissue function. As described in Figure 8A–E, the levels of AST, ALT, BUN, and creatinine were significantly increased after LPS induction compared with that of the control group. However, the enhancement of these indices was significantly reversed after treatment with different concentrations of D25 and DEX, which means that our inhibitor D25 could protect the tissues from an inflammation response induced by LPS.

The release of a large number of inflammatory factors into the circulatory system is a major response of sepsis induced by LPS. We then tested various pro-inflammatory cytokines in serum from each group. There was a substantial rise in serum TNF- α , IL-1 β , and IL-6 after the induction of LPS compared to the control group (Figure 9A–C). Importantly, these increased inflammatory cytokines were significantly suppressed in the LPS + D25 (20 mg/kg) and LPS + DEX (2.5 mg/kg) groups. We also tested the protein level of p-eIF4E, i-NOS, COX-2, TNF- α , and IL-6 from spleen tissue. We found that the LPS alone group had a higher level of these pro-inflammatory cytokines, and D25 inhibited the induction of these proteins significantly (Figure 9D,E). Furthermore, D25 and DEX could decrease the infiltration of macrophages in spleen induced by LPS (Figure 9F,G). The results showed that D25 inhibited the release of pro-inflammatory cytokines induced by LPS and the activity of MNKs to improve sepsis-associated ASI.

It has been demonstrated that administering LPS intraperitoneally decreases antioxidant enzymes such as GST, GSH, and SOD and significantly increases oxidative stress markers

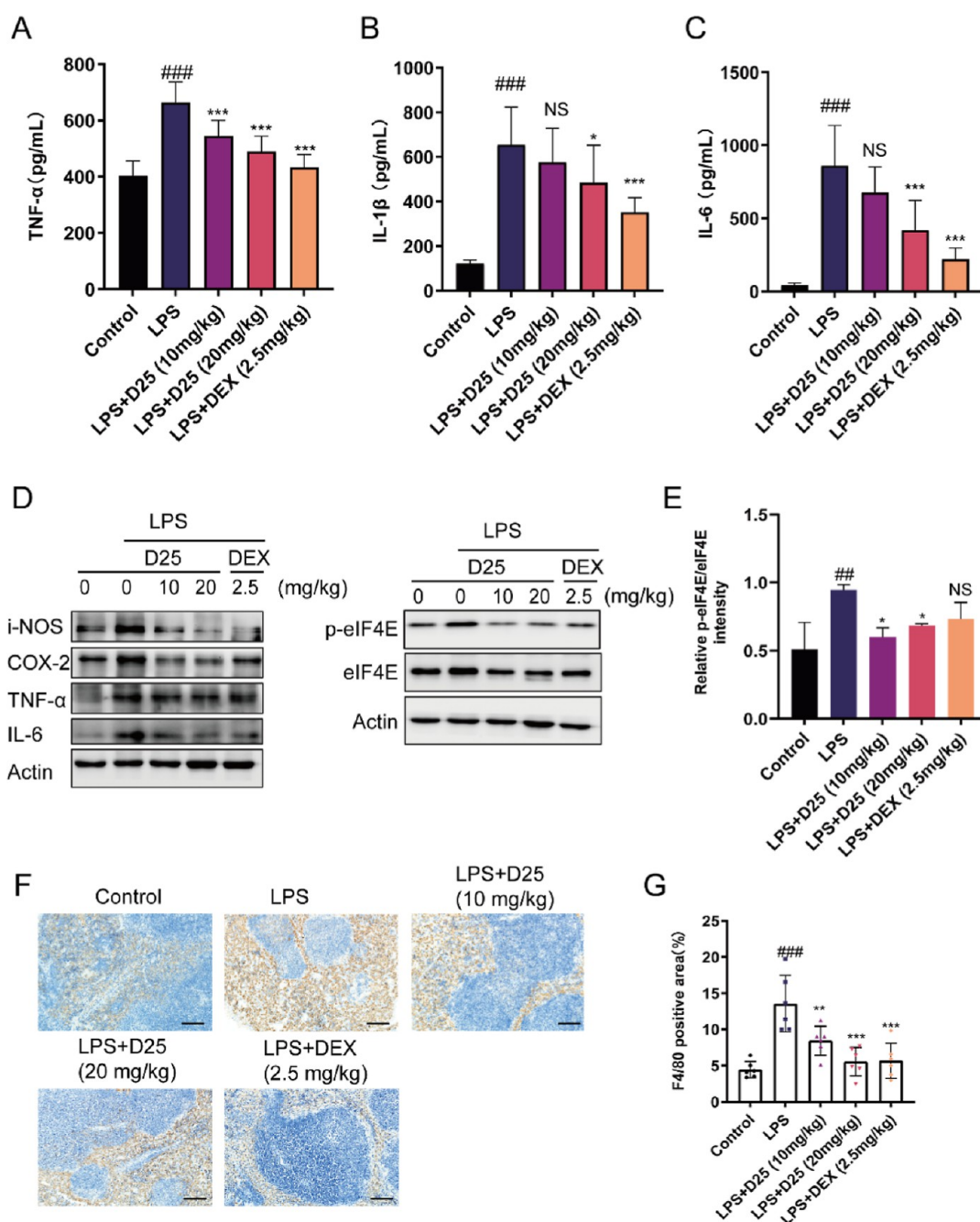


Figure 9. D25 reduces the expression of inflammatory factors in LPS-induced ASI mice. (A–C) Levels of TNF- α , IL-1 β , and IL-6 in serum, $n = 8$. (D) Western blot analysis of the indicated protein expression from spleen tissue of each group. (E) Quantification of p-eIF4E/eIF4E from (D). (F,G) Representative photos of IHC analysis for F4/80 (macrophages) in the spleen tissue from each group and quantification of the F4/80-positive area ($n = 6$, magnification: 200 \times , scale bar: 100 μ m). ### $p < 0.01$, #### $p < 0.001$ vs controls; * $p < 0.05$, ** $p < 0.01$, and *** $p < 0.001$ vs LPS-treated cells.

production such as POD and MDA in vivo.³⁷ Therefore, we examined the antioxidant enzyme activity (SOD and GSH) and MDA, a marker of lipid peroxidation. In comparison to the control group, the level of MDA was increased (Figure 10A), and the levels of SOD and GSH were decreased after LPS treatment (Figure 10B,C). These changes were reversed after D25 (20 mg/kg) and DEX treatment. The development of inflammatory events increased the production and release of cellular ROS, exacerbating oxidative stress and its consequent tissue damage. We found that an increased level of ROS with LPS stimulation could be reduced with D25 and DEX, which indicated that D25 provided relief for the excessive inflamma-

tory response and then reduced the release of ROS to improve subsequent oxidative stress (Figure 10D,E).

Pharmacokinetics. Since D25 could be a potent MNK inhibitor with good in vivo anti-inflammation activity induced by LPS, we further carried out a pharmacokinetics (PK) study on D25 (Table S2). After intravenous (i.v.) administration of 5 mg/kg D25, the maximum concentration (C_{max}), area under the curve (AUC_{0-t}), half-life ($t_{1/2}$), and clearance rate (CL) values were 3577 ng/mL, 1618 ng-h/mL, 5.52 h, and 3118 mL/h/kg, respectively. However, after oral administration (p.o.) at 20 mg/kg, a poor PK profile with a C_{max} of 26.2 ng/mL, a AUC_{0-t} of 75.3 ng-h/mL, a $t_{1/2}$ of 3.34 h, and a F (%) of 1.16 were found.

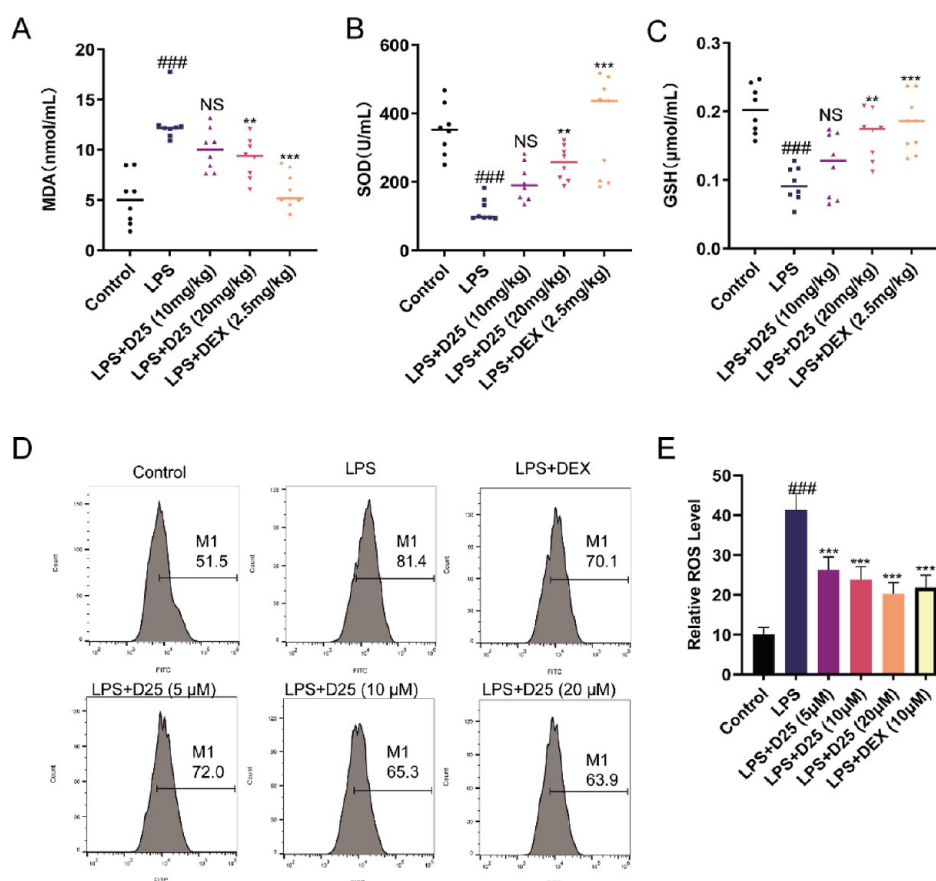


Figure 10. Effect of D25 on oxidative stress induced by LPS. (A–C) Levels of MDA, SOD, and GSH in serum, $n = 8$. (D,E) ROS level of each group after LPS was induced in RAW264.7 cells. ### $p < 0.001$ vs controls; ** $p < 0.01$, and *** $p < 0.001$ vs LPS-treated cells.

We assumed that D25 may be metabolized soon in the liver. Although D25 has a low bioavailability with oral administration, it still showed a satisfactory activity *in vivo*. Improving the oral bioavailability of D25 is a major challenge in subsequent research, as it dictates the efficiency and efficacy of drug absorption into the systemic circulation after oral administration. The following strategies could be used to enhance the oral bioavailability of D25: (1) generate pharmaceutically acceptable salts to improve solubility and dissolution rate; (2) minimize sites of metabolic vulnerability to reduce first-pass metabolism; (3) oral administration was changed to intravenous administration.

CONCLUSIONS

Here, we have characterized a series of new MNK inhibitors based on a 4-(3-(piperidin-4-yl)-1*H*-pyrazol-5-yl)pyridine scaffold. Structure-guided modification of compound **1** led to compound D25 with good selectivity against a panel of 70 kinases and increased MNK inhibitory activity with IC_{50} values of 120.6 nM for MNK1 and 134.7 nM for MNK2. Moreover, D25 exerted good anti-inflammation effects on RAW264.7 cells and sepsis-associated ASI induced by LPS by reducing the expression of proinflammatory cytokines TNF- α , IL-6, COX-2, and i-NOS and inhibiting the production of ROS to relieve oxidative stress. In conclusion, our findings demonstrate the potential of D25 as a potent MNK inhibitor, providing a promising therapeutic approach for inflammatory diseases.

EXPERIMENTAL SECTION

Chemistry. Compound Synthesis. All reagents and solvents were purchased from Aladdin, Energy Chemical, Bide Chemical, or Tian jin heng xing Chemical, and all were reagent grade quality. All actions were carried out with continuous magnetic stirring in common glassware. Cooling of reactions was conducted with ice or an ice bath. 1H and ^{13}C spectra were measured on a Bruker 600 or 500 NMR spectrometer (1H at 600 MHz and ^{13}C at 150 MHz; 1H at 500 MHz and ^{13}C at 125 MHz) with tetramethylsilane (Me_4Si) as the internal standard, chemical shifts were reported as δ values (ppm) with $CDCl_3$ (1H : $\delta = 7.26$, ^{13}C : $\delta = 77.16$) or $DMSO-d_6$ (1H : $\delta = 2.50$, ^{13}C : $\delta = 39.52$) as the internal standard. Mass spectra were measured on a Q-TOF Global mass spectrometer. Column chromatography was performed on silica gel (200–300 mesh, Qingdao, China). The docking soft is MOE. The high-performance liquid chromatography (HPLC) analysis conditions were as follows: column: ZORBAX SB-C18 (4.6 mm \times 250 mm); flow rate: 0.5 mL/min; detection: 254 nm; eluent A: water and 0.1% trifluoroacetic acid; eluent B: methanol. All target compounds were found to display >95% purity.

General Procedure for 1–37. A mixture of substituted aromatic aldehydes (1 equiv) and 3-quinuclidinone hydrochloride (1 equiv) was stirred in the presence of NaOH (1.1 equiv) in EtOH and subjected to reflux for 3 h. After the reaction, the mixture was concentrated under reduced pressure, washed with water, and extracted with EA three times. The organic layer was concentrated to get a yellow solid (compounds **1a–37a**). Then, **1a–37a** without further purification (100 mg) was refluxed with 20% hydrazine hydrate (3 mL) for 6 h or until a solid precipitate was observed forming in the reaction mixture. Following completion of the reaction, the mixture was filtered, and the resultant solid was washed with water and diethyl ether to afford the desired target compounds **1–37** in a purified state.

4-(3-(Piperidin-4-yl)-1H-pyrazol-5-yl)pyridine (1). 4-Pyridinecarboxaldehyde (133 mg, 1.24 mmol) was reacted with 3-quinuclidinone hydrochloride and hydrazine hydrate according to the general procedure. Compound **1** was yielded as a white solid of 49%. ^1H NMR (600 MHz, DMSO- d_6): δ 12.95 (s, 1H), 8.57–8.54 (m, 2H), 7.74–7.72 (m, 2H), 6.66 (s, 1H), 2.99 (dt, $J = 12.3, 3.3$ Hz, 2H), 2.73 (tt, $J = 11.8, 3.8$ Hz, 1H), 2.56 (td, $J = 12.0, 2.4$ Hz, 2H), 1.88–1.82 (m, 2H), 1.51 (qd, $J = 12.2, 3.9$ Hz, 2H). ^{13}C NMR (150 MHz, DMSO- d_6): δ 151.19, 150.50, 147.23, 140.97, 119.84, 100.27, 46.48, 34.35, 33.19. HRMS calcd for (M + H) $^+$, 229.1483; found, 229.1485.

4-(5-Phenyl-1H-pyrazol-3-yl)piperidine (2). Benzaldehyde (328 mg, 3.09 mmol) was reacted with 3-quinuclidinone hydrochloride and hydrazine hydrate according to the general procedure. Compound **2** was yielded as a white solid of 75%. ^1H NMR (500 MHz, DMSO- d_6): δ 12.62 (s, 1H), 7.74 (d, $J = 7.5$ Hz, 2H), 7.37 (t, $J = 7.6$ Hz, 2H), 7.26 (t, $J = 7.3$ Hz, 1H), 6.45 (s, 1H), 3.01–2.93 (m, 2H), 2.68 (ddd, $J = 11.7, 8.3, 3.7$ Hz, 1H), 2.55 (td, $J = 12.0, 2.2$ Hz, 2H), 2.00 (dd, $J = 14.9, 7.2$ Hz, 1H), 1.83 (d, $J = 10.6$ Hz, 2H), 1.50 (qd, $J = 12.2, 3.8$ Hz, 2H). ^{13}C NMR (125 MHz, DMSO- d_6): δ 129.0, 127.6, 125.4, 99.1, 46.56, 33.32. HRMS calcd for (M + H) $^+$, 228.1495; found, 228.1492.

4-(5-(3-Fluorophenyl)-1H-pyrazol-3-yl)piperidine (3). 3-Fluorobenzaldehyde (330.3 mg, 2.66 mmol) was reacted with 3-quinuclidinone hydrochloride and hydrazine hydrate according to the general procedure. Compound **3** was yielded as a white solid of 54%. ^1H NMR (500 MHz, DMSO- d_6): δ 12.73 (s, 1H), 7.60 (d, $J = 7.7$ Hz, 1H), 7.54 (d, $J = 10.4$ Hz, 1H), 7.41 (dd, $J = 14.3, 7.8$ Hz, 1H), 7.08 (dd, $J = 11.8, 5.2$ Hz, 1H), 6.53 (s, 1H), 2.99 (d, $J = 12.1$ Hz, 2H), 2.73–2.65 (m, 1H), 2.56 (t, $J = 11.3$ Hz, 2H), 1.83 (d, $J = 11.6$ Hz, 2H), 1.50 (qd, $J = 12.3, 3.6$ Hz, 2H). ^{13}C NMR (125 MHz, DMSO- d_6): δ 163.9, 162.0, 131.0 (d, $J = 8.6$ Hz), 121.4 (d, $J = 2.3$ Hz), 114.2 (d, $J = 21.1$ Hz), 111.8 (d, $J = 22.5$ Hz), 99.6, 46.4, 34.4, 33.0. HRMS calcd for (M + H) $^+$, 246.1401; found, 246.1404.

4-(5-(4-Fluorophenyl)-1H-pyrazol-3-yl)piperidine (4). 4-Fluorobenzaldehyde (154 mg, 1.24 mmol) was reacted with 3-quinuclidinone hydrochloride and hydrazine hydrate according to the general procedure. Compound **4** was yielded as a white solid of 65%. ^1H NMR (400 MHz, DMSO- d_6): δ 12.58 (s, 1H), 7.83–7.76 (m, 2H), 7.22 (t, $J = 8.9$ Hz, 2H), 6.46 (d, $J = 4.0$ Hz, 1H), 2.99 (d, $J = 12.1$ Hz, 2H), 2.70 (ddd, $J = 11.7, 8.2, 3.8$ Hz, 1H), 2.61–2.52 (m, 2H), 1.84 (d, $J = 12.5$ Hz, 2H), 1.51 (qd, $J = 12.3, 3.8$ Hz, 2H). ^{13}C NMR (100 MHz, DMSO- d_6): δ 163.2, 160.7, 127.3 (d, $J = 8.0$ Hz), 116.0, 115.8, 99.0, 46.5, 33.2, 31.8. HRMS calcd for (M + H) $^+$, 246.1401; found, 246.1405.

4-(3-(Piperidin-4-yl)-1H-pyrazol-5-yl)benzotrile (5). 4-Cyanobenzaldehyde (242.6 mg, 1.85 mmol) was reacted with 3-quinuclidinone hydrochloride and hydrazine hydrate according to the general procedure. Compound **5** was yielded as a yellow solid of 52%. ^1H NMR (400 MHz, DMSO- d_6): δ 12.92 (s, 1H), 7.96 (d, $J = 8.4$ Hz, 2H), 7.84 (d, $J = 8.4$ Hz, 2H), 6.64 (s, 1H), 2.99 (d, $J = 12.1$ Hz, 2H), 2.72 (ddd, $J = 15.4, 7.8, 3.7$ Hz, 1H), 2.61–2.52 (m, 2H), 2.02 (dd, $J = 53.6, 45.8$ Hz, 1H), 1.84 (d, $J = 10.6$ Hz, 2H), 1.51 (qd, $J = 12.2, 3.8$ Hz, 2H). ^{13}C NMR (100 MHz, DMSO- d_6): δ 133.1, 125.9, 119.5, 109.8, 100.3, 46.5, 34.3, 33.2. HRMS calcd for (M + H) $^+$, 253.1448; found, 253.1448.

4-(5-(4-Nitrophenyl)-1H-pyrazol-3-yl)piperidine (6). 4-Nitrobenzaldehyde (279.5 mg, 1.85 mmol) was reacted with 3-quinuclidinone hydrochloride and hydrazine hydrate according to the general procedure. Compound **6** was yielded as a yellow solid of 52%. ^1H NMR (400 MHz, DMSO- d_6): δ 13.01 (s, 1H), 8.25 (d, $J = 8.9$ Hz, 2H), 8.04 (d, $J = 8.9$ Hz, 2H), 6.69 (s, 1H), 3.00 (d, $J = 12.1$ Hz, 2H), 2.73 (tt, $J = 11.6, 3.5$ Hz, 1H), 2.57 (td, $J = 11.9, 1.9$ Hz, 2H), 2.03 (dd, $J = 22.9, 15.5$ Hz, 1H), 1.86 (d, $J = 10.7$ Hz, 2H), 1.51 (qd, $J = 12.3, 3.8$ Hz, 2H). ^{13}C NMR (100 MHz, DMSO- d_6): δ 151.4, 147.8, 146.6, 140.6, 126.1, 124.6, 100.6, 46.5, 34.3, 33.1. HRMS calcd for (M + H) $^+$, 273.1346; found, 273.1349.

4-(5-(4-(Trifluoromethyl)phenyl)-1H-pyrazol-3-yl)piperidine (7). 4-(Trifluoromethyl)benzaldehyde (434 mg, 2.49 mmol) was reacted with 3-quinuclidinone hydrochloride and hydrazine hydrate according to the general procedure. Compound **7** was yielded as a yellow solid of 86%. ^1H NMR (600 MHz, DMSO- d_6): δ 12.82 (s, 1H), 7.99 (d, $J = 7.9$ Hz, 2H), 7.74 (d, $J = 8.0$ Hz, 2H), 6.61 (s, 1H), 3.01 (d, $J = 11.9$ Hz,

2H), 2.73 (d, $J = 14.6$ Hz, 1H), 2.58 (t, $J = 11.8$ Hz, 3H), 1.86 (d, $J = 12.6$ Hz, 2H), 1.52 (qd, $J = 12.2, 3.8$ Hz, 2H). ^{13}C NMR (150 MHz, DMSO- d_6): δ 158.92, 158.71, 158.50, 126.12, 125.96, 125.72, 123.91, 120.71, 118.72, 116.73, 43.31, 30.79, 28.44. HRMS calcd for (M + H) $^+$, 296.1374; found, 296.1373.

1-Methyl-4-(4-(3-(piperidin-4-yl)-1H-pyrazol-5-yl)phenyl)piperazine (8). 4-(4-Methylpiperazino)benzaldehyde (233 mg, 1.14 mmol) was reacted with 3-quinuclidinone hydrochloride and hydrazine hydrate according to the general procedure. Compound **8** was yielded as a yellow solid of 65%. ^1H NMR (500 MHz, DMSO- d_6): δ 13.01 (s, 1H), 7.56 (d, $J = 8.6$ Hz, 2H), 6.93 (d, $J = 8.5$ Hz, 2H), 6.30 (s, 1H), 3.30 (s, 4H), 2.98 (d, $J = 9.1$ Hz, 2H), 2.65 (s, 1H), 2.55 (s, 2H), 2.46–2.41 (m, 4H), 2.21 (s, 3H), 1.82 (d, $J = 11.9$ Hz, 2H), 1.49 (qd, $J = 12.3, 3.7$ Hz, 2H). ^{13}C NMR (125 MHz, DMSO- d_6): δ 150.6, 126.2, 115.6, 98.2, 55.0, 48.3, 46.5, 46.2, 33.3. HRMS calcd for (M + H) $^+$, 326.2339; found, 326.2335.

4-(5-(4-Fluoro-2-methylphenyl)-1H-pyrazol-3-yl)piperidine (9). 4-Fluoro-2-methylbenzaldehyde (170 mg, 1.23 mmol) was reacted with 3-quinuclidinone hydrochloride and hydrazine hydrate according to the general procedure. Compound **9** was yielded as a yellow solid of 35%. ^1H NMR (600 MHz, DMSO- d_6): δ 12.65 (s, 1H), 7.51 (t, $J = 7.4$ Hz, 1H), 7.12 (d, $J = 10.1$ Hz, 1H), 7.07–7.01 (m, 1H), 6.25 (s, 1H), 3.03 (d, $J = 12.0$ Hz, 2H), 2.74 (tt, $J = 12.0, 3.8$ Hz, 1H), 2.62 (t, $J = 12.0$ Hz, 2H), 2.39 (s, 3H), 1.88 (dd, $J = 13.2, 3.5$ Hz, 2H), 1.55 (qd, $J = 12.3, 3.8$ Hz, 2H). ^{13}C NMR (150 MHz, DMSO- d_6): δ 162.45, 160.83, 138.49, 138.44, 131.00, 130.95, 117.58, 117.44, 113.02, 112.88, 101.97, 46.17, 32.72, 21.53. HRMS calcd for (M + H) $^+$, 260.1558; found, 260.1561.

4-(5-(3,5-Difluorophenyl)-1H-pyrazol-3-yl)piperidine (10). 3,5-Difluorobenzaldehyde (174.8 mg, 1.23 mmol) was reacted with 3-quinuclidinone hydrochloride and hydrazine hydrate according to the general procedure. Compound **10** was yielded as a yellow solid of 35%. ^1H NMR (600 MHz, DMSO- d_6): δ 12.84 (s, 1H), 7.49–7.44 (m, 2H), 7.11 (tt, $J = 9.3, 2.5$ Hz, 1H), 6.62 (s, 1H), 2.99 (d, $J = 12.0$ Hz, 2H), 2.71 (tt, $J = 11.9, 3.8$ Hz, 1H), 2.60–2.53 (m, 2H), 1.84 (dd, $J = 12.4, 3.1$ Hz, 2H), 1.50 (qd, $J = 12.2, 3.9$ Hz, 2H). ^{13}C NMR (150 MHz, DMSO- d_6): δ 164.10, 164.01, 162.48, 162.39, 108.28, 108.25, 108.14, 108.11, 102.87, 102.69, 102.52, 100.05, 46.41, 34.30, 33.11. HRMS calcd for (M + H) $^+$, 264.1352; found, 264.1354.

4-(5-(3,4-Difluorophenyl)-1H-pyrazol-3-yl)piperidine (11). 3,4-Difluorobenzaldehyde (174.8 mg, 1.23 mmol) was reacted with 3-quinuclidinone hydrochloride and hydrazine hydrate according to the general procedure. Compound **11** was yielded as a yellow solid of 54%. ^1H NMR (600 MHz, DMSO- d_6): δ 13.01 (s, 1H), 7.80 (ddd, $J = 12.1, 7.8, 2.1$ Hz, 1H), 7.63 (ddd, $J = 9.5, 4.7, 2.2$ Hz, 1H), 7.48 (dt, $J = 10.6, 8.6$ Hz, 1H), 6.62 (s, 1H), 3.35 (dt, $J = 12.5, 3.2$ Hz, 2H), 3.08–2.95 (m, 3H), 2.12 (dd, $J = 14.2, 3.6$ Hz, 2H), 1.82–1.74 (m, 2H). ^{13}C NMR (150 MHz, DMSO- d_6): δ 158.92, 158.71, 158.49, 158.27, 151.02, 150.93, 150.11, 150.03, 149.40, 149.31, 148.48, 148.40, 122.20, 122.18, 122.16, 122.14, 118.42, 118.30, 116.20, 114.38, 114.26, 100.10, 43.32, 31.43, 28.45. HRMS calcd for (M + H) $^+$, 264.1352; found, 264.1354.

4-(5-(3,4,5-Trifluorophenyl)-1H-pyrazol-3-yl)piperidine (12). 3,4,5-Trifluorobenzaldehyde (395.2 mg, 2.46 mmol) was reacted with 3-quinuclidinone hydrochloride and hydrazine hydrate according to the general procedure. Compound **12** was yielded as a yellow solid of 63%. ^1H NMR (600 MHz, DMSO- d_6): δ 12.83 (s, 1H), 7.70–7.63 (m, 2H), 6.61 (s, 1H), 2.99 (dt, $J = 12.3, 3.4$ Hz, 2H), 2.70 (ddt, $J = 11.8, 7.7, 3.8$ Hz, 1H), 2.56 (td, $J = 12.0, 2.5$ Hz, 2H), 1.83 (dd, $J = 13.4, 3.6$ Hz, 2H), 1.49 (qd, $J = 12.2, 3.9$ Hz, 2H). ^{13}C NMR (150 MHz, DMSO- d_6): δ 151.90, 151.85, 150.26, 150.19, 139.11, 139.00, 137.46, 131.21 (d, $J = 17.7$ Hz), 109.65, 109.62, 109.53, 109.51, 99.89, 46.43, 34.25, 33.15. HRMS calcd for (M + H) $^+$, 282.1258; found, 282.1260.

4-(5-(2,4-Difluorophenyl)-1H-pyrazol-3-yl)piperidine (13). 2,4-Difluorobenzaldehyde (174.8 mg, 1.23 mmol) was reacted with 3-quinuclidinone hydrochloride and hydrazine hydrate according to the general procedure. Compound **13** was yielded as a yellow solid of 54%. ^1H NMR (600 MHz, DMSO- d_6): δ 12.83 (s, 1H), 7.94 (q, $J = 8.2$ Hz, 1H), 7.30 (ddd, $J = 11.6, 9.3, 2.6$ Hz, 1H), 7.14 (td, $J = 8.4, 2.6$ Hz, 1H), 6.37 (d, $J = 3.7$ Hz, 1H), 3.00 (d, $J = 12.0$ Hz, 2H), 2.78–2.70 (m, 1H), 2.58 (t, $J = 12.0$ Hz, 2H), 1.85 (dd, $J = 12.9, 3.7$ Hz, 2H), 1.52 (qd, $J =$

12.2, 4.0 Hz, 2H). ^{13}C NMR (150 MHz, DMSO- d_6): δ 162.65, 162.57, 161.02, 160.93, 160.33, 158.66, 158.58, 129.64, 129.60, 129.57, 129.54, 112.42, 112.39, 112.28, 112.25, 105.08, 104.90, 104.73, 101.75, 46.34, 34.22, 33.00. HRMS calcd for (M + H) $^+$, 264.1307; found, 264.1308.

3-(3-(Piperidin-4-yl)-1H-pyrazol-5-yl)pyridine (14). 3-Pyridinecarboxaldehyde (131.7 mg, 1.23 mmol) was reacted with 3-quinuclidinone hydrochloride and hydrazine hydrate according to the general procedure. Compound **14** was yielded as a yellow solid of 67%. ^1H NMR (600 MHz, DMSO- d_6): δ 12.81 (s, 1H), 8.99 (d, J = 2.2 Hz, 1H), 8.48 (dd, J = 4.8, 1.7 Hz, 1H), 8.12 (dt, J = 7.9, 2.0 Hz, 1H), 7.41 (dd, J = 7.9, 4.7 Hz, 1H), 6.59 (s, 1H), 2.99 (dt, J = 12.2, 3.3 Hz, 2H), 2.72 (tt, J = 11.8, 3.8 Hz, 1H), 2.57 (td, J = 12.0, 2.4 Hz, 2H), 1.87–1.81 (m, 2H), 1.52 (qd, J = 12.2, 3.9 Hz, 2H). ^{13}C NMR (150 MHz, DMSO- d_6): δ 148.65, 146.76, 132.53, 124.20, 99.51, 46.50, 34.42, 33.23. HRMS calcd for (M + H) $^+$, 229.1483; found, 229.1485.

5-(3-(Piperidin-4-yl)-1H-pyrazol-5-yl)pyrimidine (15). Pyrimidine-5-carboxaldehyde (133 mg, 1.23 mmol) was reacted with 3-quinuclidinone hydrochloride and hydrazine hydrate according to the general procedure. Compound **15** was yielded as a yellow solid of 47%. ^1H NMR (600 MHz, DMSO- d_6): δ 12.98 (s, 1H), 9.16 (s, 2H), 9.10 (s, 1H), 6.70 (s, 1H), 3.00 (dt, J = 12.3, 3.3 Hz, 2H), 2.74 (tt, J = 11.8, 3.8 Hz, 1H), 2.57 (td, J = 12.1, 2.5 Hz, 2H), 1.88–1.82 (m, 2H), 1.51 (qd, J = 12.2, 3.9 Hz, 2H). ^{13}C NMR (150 MHz, DMSO- d_6): δ 157.46, 153.48, 127.91, 99.94, 46.44, 34.23, 33.17. HRMS calcd for (M + H) $^+$, 230.1405; found, 230.1406.

2-(3-(Piperidin-4-yl)-1H-pyrazol-5-yl)pyrazine (16). Pyrazine-2-carboxaldehyde (133.5 mg, 1.23 mmol) was reacted with 3-quinuclidinone hydrochloride and hydrazine hydrate according to the general procedure. Compound **16** was yielded as a yellow solid of 37%. ^1H NMR (600 MHz, DMSO- d_6): δ 13.05 (s, 1H), 9.14 (d, J = 1.5 Hz, 1H), 8.61 (t, J = 1.9 Hz, 1H), 8.52 (d, J = 2.6 Hz, 1H), 6.67 (s, 1H), 2.99 (dt, J = 12.3, 3.3 Hz, 2H), 2.75 (tt, J = 11.9, 3.9 Hz, 1H), 2.57 (td, J = 12.0, 2.5 Hz, 2H), 1.89–1.82 (m, 2H), 1.52 (qd, J = 12.2, 3.9 Hz, 2H). ^{13}C NMR (150 MHz, DMSO- d_6): δ 147.97, 144.54, 143.40, 141.57, 101.03, 46.48, 34.35, 33.17. HRMS calcd for (M + H) $^+$, 230.1400; found, 230.1404.

4-(3-(Piperidin-4-yl)-1H-pyrazol-5-yl)pyrimidine (17). Pyrimidine-4-carboxaldehyde (133 mg, 1.23 mmol) was reacted with 3-quinuclidinone hydrochloride and hydrazine hydrate according to the general procedure. Compound **17** was yielded as a yellow solid of 32%. ^1H NMR (600 MHz, DMSO- d_6): δ 9.17 (d, J = 1.4 Hz, 1H), 8.81 (d, J = 5.3 Hz, 1H), 7.93 (dd, J = 5.3, 1.4 Hz, 1H), 6.84 (s, 1H), 3.36 (dt, J = 12.7, 3.2 Hz, 2H), 3.10–3.01 (m, 3H), 2.15 (dd, J = 14.3, 3.7 Hz, 2H), 1.85–1.76 (m, 2H). ^{13}C NMR (150 MHz, DMSO- d_6): δ 163.96, 163.89, 162.84, 122.35, 121.33, 120.41, 107.06, 48.08, 36.12, 33.15. HRMS calcd for (M + H) $^+$, 230.1400; found, 230.1400.

4-(5-(Thiophen-3-yl)-1H-pyrazol-3-yl)piperidine (18). 3-Thiophenecarboxaldehyde (137 mg, 1.23 mmol) was reacted with 3-quinuclidinone hydrochloride and hydrazine hydrate according to the general procedure. Compound **18** was yielded as a yellow solid of 45%. ^1H NMR (600 MHz, DMSO- d_6): δ 12.50 (s, 1H), 7.70 (s, 1H), 7.56 (t, J = 3.8 Hz, 1H), 7.45 (dd, J = 5.0, 1.2 Hz, 1H), 6.35 (s, 1H), 2.99 (dt, J = 12.2, 3.4 Hz, 2H), 2.71–2.65 (m, 1H), 2.56 (td, J = 12.0, 2.5 Hz, 2H), 1.85–1.80 (m, 2H), 1.49 (qd, J = 12.2, 3.9 Hz, 2H). ^{13}C NMR (150 MHz, DMSO- d_6): δ 126.96, 126.29, 120.34, 99.45, 46.55, 34.05, 33.35. HRMS calcd for (M + H) $^+$, 234.1060; found, 234.1062.

5-(3-(Piperidin-4-yl)-1H-pyrazol-5-yl)thiazole (19). 1,3-Thiazole-2-carboxaldehyde (138 mg, 1.23 mmol) was reacted with 3-quinuclidinone hydrochloride and hydrazine hydrate according to the general procedure. Compound **19** was yielded as a yellow solid of 72%. ^1H NMR (600 MHz, DMSO- d_6): δ 12.82 (s, 1H), 8.98 (s, 1H), 8.17 (s, 1H), 6.48 (s, 1H), 3.09 (dt, J = 12.5, 3.4 Hz, 2H), 2.80 (tt, J = 11.7, 3.8 Hz, 1H), 2.70 (td, J = 12.2, 2.6 Hz, 2H), 1.95–1.89 (m, 2H), 1.57 (qd, J = 12.3, 3.9 Hz, 2H). ^{13}C NMR (150 MHz, DMSO- d_6): δ 158.39, 153.00, 150.17, 139.67, 132.54, 99.85, 45.48, 33.18, 31.69. HRMS calcd for (M + H) $^+$, 235.1012; found, 235.1012.

2-Methyl-4-(3-(piperidin-4-yl)-1H-pyrazol-5-yl)pyridine (20). 3-Methyl-4-pyridinecarboxaldehyde (150 mg, 1.23 mmol) was reacted with 3-quinuclidinone hydrochloride and hydrazine hydrate according

to the general procedure. Compound **20** was yielded as a yellow solid of 76%. ^1H NMR (600 MHz, DMSO- d_6): δ 12.91 (s, 1H), 8.42 (d, J = 5.2 Hz, 1H), 7.61 (d, J = 1.6 Hz, 1H), 7.52 (dd, J = 5.2, 1.6 Hz, 1H), 6.63 (s, 1H), 2.99 (dt, J = 12.3, 3.3 Hz, 2H), 2.72 (tt, J = 11.8, 3.9 Hz, 1H), 2.56 (td, J = 12.0, 2.4 Hz, 2H), 2.49 (s, 3H), 1.87–1.81 (m, 2H), 1.50 (qd, J = 12.2, 3.9 Hz, 2H). ^{13}C NMR (150 MHz, DMSO- d_6): δ 158.70, 149.78, 119.02, 117.11, 100.20, 46.48, 34.36, 33.19, 24.58. HRMS calcd for (M + H) $^+$, 243.1604; found, 243.1607.

2,6-Dimethyl-4-(3-(piperidin-4-yl)-1H-pyrazol-5-yl)pyridine (21). 2,6-Dimethylpyridine-4-carboxaldehyde (166.2 mg, 1.23 mmol) was reacted with 3-quinuclidinone hydrochloride and hydrazine hydrate according to the general procedure. Compound **21** was yielded as a yellow solid of 64%. ^1H NMR (600 MHz, DMSO- d_6): δ 12.87 (s, 1H), 7.40 (s, 2H), 6.59 (s, 1H), 2.99 (dt, J = 12.2, 3.3 Hz, 2H), 2.71 (tt, J = 11.8, 3.8 Hz, 1H), 2.56 (td, J = 12.0, 2.4 Hz, 2H), 2.44 (s, 6H), 1.87–1.82 (m, 2H), 1.54–1.46 (m, 2H). ^{13}C NMR (150 MHz, DMSO- d_6): δ 162.67, 156.28, 152.49, 146.27, 121.00, 104.90, 51.23, 39.13, 37.95, 29.26. HRMS calcd for (M + H) $^+$, 257.1761; found, 257.1763.

3-Fluoro-4-(3-(piperidin-4-yl)-1H-pyrazol-5-yl)pyridine (22). 3-Fluoropyridine-4-carboxaldehyde (153.7 mg, 1.23 mmol) was reacted with 3-quinuclidinone hydrochloride and hydrazine hydrate according to the general procedure. Compound **22** was yielded as a yellow solid of 37%. ^1H NMR (600 MHz, DMSO- d_6): δ 13.16 (s, 1H), 8.60 (d, J = 2.8 Hz, 1H), 8.42 (dd, J = 5.1, 1.1 Hz, 1H), 7.92 (dd, J = 6.7, 5.0 Hz, 1H), 6.55 (d, J = 3.7 Hz, 1H), 2.99 (dt, J = 12.2, 3.3 Hz, 2H), 2.76 (tt, J = 11.8, 3.8 Hz, 1H), 2.56 (td, J = 12.1, 2.5 Hz, 2H), 1.88–1.82 (m, 2H), 1.51 (qd, J = 12.2, 3.9 Hz, 2H). ^{13}C NMR (150 MHz, DMSO- d_6): δ 157.00, 155.30, 151.10, 146.43, 146.40, 141.91, 139.34, 139.18, 128.54, 128.48, 121.53, 103.23, 103.17, 46.45, 34.18, 33.13. HRMS calcd for (M + H) $^+$, 247.1354; found, 247.1356.

2-Fluoro-4-(3-(piperidin-4-yl)-1H-pyrazol-5-yl)pyridine (23). 2-Fluoropyridine-4-carboxaldehyde (153.7 mg, 1.23 mmol) was reacted with 3-quinuclidinone hydrochloride and hydrazine hydrate according to the general procedure. Compound **23** was yielded as a yellow solid of 41%. ^1H NMR (600 MHz, DMSO- d_6): δ 13.41 (s, 1H), 8.24 (d, J = 5.3 Hz, 1H), 7.75 (d, J = 5.1 Hz, 1H), 7.52 (s, 1H), 6.83 (s, 1H), 3.29–3.25 (m, 3H), 3.04–2.94 (m, 3H), 2.12 (dd, J = 14.1, 3.7 Hz, 2H), 1.86 (qd, J = 12.3, 3.9 Hz, 2H). ^{13}C NMR (150 MHz, DMSO- d_6): δ 156.99, 155.29, 151.08, 146.43, 146.40, 141.89, 139.34, 139.18, 128.54, 128.48, 121.53, 103.23, 103.17, 46.45, 34.18, 33.13. HRMS calcd for (M + H) $^+$, 247.1354; found, 247.1356.

2-Chloro-4-(3-(piperidin-4-yl)-1H-pyrazol-5-yl)pyridine (24). 2-Chloropyridine-4-carboxaldehyde (172.8 mg, 1.23 mmol) was reacted with 3-quinuclidinone hydrochloride and hydrazine hydrate according to the general procedure. Compound **24** was yielded as a yellow solid of 84%. ^1H NMR (600 MHz, DMSO- d_6): δ 13.23 (s, 1H), 8.41 (d, J = 5.2 Hz, 1H), 7.86 (s, 1H), 7.79 (d, J = 5.2 Hz, 1H), 6.87 (s, 1H), 3.05 (td, J = 12.6, 6.5 Hz, 3H), 2.14 (dd, J = 14.5, 3.8 Hz, 2H), 1.84–1.74 (m, 2H). ^{13}C NMR (150 MHz, DMSO- d_6): δ 151.52, 150.76, 119.70, 119.20, 100.99, 46.38, 34.17, 33.05. HRMS calcd for (M + H) $^+$, 263.1083; found, 263.1087.

3-Chloro-4-(3-(piperidin-4-yl)-1H-pyrazol-5-yl)pyridine (25). 3-Chloropyridine-4-carboxaldehyde (172.8 mg, 1.23 mmol) was reacted with 3-quinuclidinone hydrochloride and hydrazine hydrate according to the general procedure. Compound **25** was yielded as a yellow solid of 84%. ^1H NMR (600 MHz, DMSO- d_6): δ 13.16 (s, 1H), 8.66 (s, 1H), 8.50 (d, J = 5.1 Hz, 1H), 7.86 (d, J = 5.1 Hz, 1H), 6.73 (s, 1H), 2.99 (dt, J = 12.4, 3.3 Hz, 2H), 2.77 (tt, J = 11.8, 3.8 Hz, 1H), 2.57 (td, J = 12.1, 2.4 Hz, 2H), 1.87–1.83 (m, 2H), 1.49 (qd, J = 12.2, 3.9 Hz, 2H). ^{13}C NMR (150 MHz, DMSO- d_6): δ 150.74, 150.46, 148.36, 144.84, 139.37, 128.30, 123.60, 103.35, 46.45, 34.18, 33.14. HRMS calcd for (M + H) $^+$, 263.1083; found, 263.1089.

2,6-Dichloro-4-(3-(piperidin-4-yl)-1H-pyrazol-5-yl)pyridine (26). 2,6-Dichloropyridine-4-carboxaldehyde (216.5 mg, 1.23 mmol) was reacted with 3-quinuclidinone hydrochloride and hydrazine hydrate according to the general procedure. Compound **26** was yielded as a yellow solid of 44%. ^1H NMR (600 MHz, DMSO- d_6): δ 13.18 (s, 1H), 7.88 (d, J = 1.6 Hz, 2H), 6.87 (s, 1H), 3.00 (dt, J = 12.4, 3.4 Hz, 2H), 2.77–2.70 (m, 1H), 2.57 (td, J = 12.0, 2.4 Hz, 2H), 1.87–1.81 (m, 2H), 1.49 (qd, J = 12.1, 3.9 Hz, 2H). ^{13}C NMR (150 MHz, DMSO- d_6): δ

151.38, 150.31, 147.67, 145.48, 118.99, 101.66, 46.30, 34.05, 32.95. HRMS calcd for (M + H)⁺, 297.0668; found, 297.0671.

3,5-Dichloro-4-(3-(piperidin-4-yl)-1H-pyrazol-5-yl)pyridine (27). 3,5-Dichloropyridine-4-carboxaldehyde (216.5 mg, 1.23 mmol) was reacted with 3-quinuclidinone hydrochloride and hydrazine hydrate according to the general procedure. Compound **27** was yielded as a yellow solid of 23%. ¹H NMR (600 MHz, DMSO-*d*₆): δ 13.03 (s, 1H), 8.71 (s, 2H), 6.25 (s, 1H), 2.99 (dt, *J* = 12.4, 3.4 Hz, 2H), 2.77 (tt, *J* = 12.1, 3.8 Hz, 1H), 2.60–2.53 (m, 2H), 1.87 (dd, *J* = 13.1, 3.6 Hz, 2H), 1.51 (qd, *J* = 12.2, 3.9 Hz, 2H). ¹³C NMR (150 MHz, DMSO-*d*₆): δ 148.28, 140.59, 132.18, 103.29, 46.44, 34.17, 33.15. HRMS calcd for (M + H)⁺, 297.0668; found, 267.0671.

2-Bromo-4-(3-(piperidin-4-yl)-1H-pyrazol-5-yl)pyridine (28). 2-Bromopyridine-4-carboxaldehyde (216.5 mg, 1.23 mmol) was reacted with 3-quinuclidinone hydrochloride and hydrazine hydrate according to the general procedure. Compound **28** was yielded as a yellow solid of 87%. ¹H NMR (600 MHz, DMSO-*d*₆): δ 13.07 (s, 1H), 8.36 (d, *J* = 5.1 Hz, 1H), 7.96 (d, *J* = 1.4 Hz, 1H), 7.79 (dd, *J* = 5.2, 1.4 Hz, 1H), 6.76 (s, 1H), 2.99 (dt, *J* = 12.3, 3.4 Hz, 2H), 2.73 (tt, *J* = 11.8, 3.8 Hz, 1H), 2.56 (td, *J* = 12.1, 2.4 Hz, 2H), 1.87–1.81 (m, 2H), 1.50 (qd, *J* = 12.1, 3.9 Hz, 2H). ¹³C NMR (150 MHz, DMSO-*d*₆): δ 151.39, 151.21, 146.10, 144.50, 142.65, 123.40, 119.49, 100.97, 46.41, 34.21, 33.10. HRMS calcd for (M + H)⁺, 307.0558; found, 307.0559.

3-Bromo-4-(3-(piperidin-4-yl)-1H-pyrazol-5-yl)pyridine (29). 3-bromopyridine-4-carboxaldehyde (216.5 mg, 1.23 mmol) was reacted with 3-quinuclidinone hydrochloride and hydrazine hydrate according to the general procedure. Compound **29** was yielded as a yellow solid of 87%. ¹H NMR (600 MHz, DMSO-*d*₆): δ 13.13 (s, 1H), 8.78 (s, 1H), 8.53 (d, *J* = 5.0 Hz, 1H), 7.78 (d, *J* = 5.0 Hz, 1H), 6.73 (s, 1H), 2.99 (dt, *J* = 12.3, 3.3 Hz, 2H), 2.77 (tt, *J* = 11.8, 3.8 Hz, 1H), 2.57 (td, *J* = 12.0, 2.4 Hz, 2H), 1.88–1.82 (m, 2H), 1.52 (qd, *J* = 12.2, 3.9 Hz, 2H). ¹³C NMR (150 MHz, DMSO-*d*₆): δ 153.21, 150.21, 148.75, 146.18, 141.53, 124.66, 118.82, 103.00, 46.44, 34.18, 33.16. HRMS calcd for (M + H)⁺, 307.0558; found, 307.0559.

2-Methoxy-4-(3-(piperidin-4-yl)-1H-pyrazol-5-yl)pyridine (30). 3-Methoxypyridine-4-carboxaldehyde (168 mg, 1.23 mmol) was reacted with 3-quinuclidinone hydrochloride and hydrazine hydrate according to the general procedure. Compound **30** was yielded as a yellow solid of 86%. ¹H NMR (600 MHz, DMSO-*d*₆): δ 12.92 (s, 1H), 8.15 (d, *J* = 5.3 Hz, 1H), 7.36 (dd, *J* = 5.4, 1.4 Hz, 1H), 7.13 (d, *J* = 1.4 Hz, 1H), 6.65 (s, 1H), 3.87 (s, 3H), 3.00 (d, *J* = 12.0 Hz, 2H), 2.73 (td, *J* = 11.5, 5.7 Hz, 1H), 2.57 (t, *J* = 11.9 Hz, 2H), 1.87–1.80 (m, 2H), 1.51 (qd, *J* = 12.2, 3.9 Hz, 2H). ¹³C NMR (150 MHz, DMSO-*d*₆): δ 164.79, 147.67, 113.98, 105.81, 100.46, 53.58, 46.36, 34.30, 33.04. HRMS calcd for (M + H)⁺, 259.1559; found, 259.1561.

4-(3-(Piperidin-4-yl)-1H-pyrazol-5-yl)-2-(trifluoromethyl)pyridine (31). 3-Trifluoromethyl-pyridine-4-carboxaldehyde (215 mg, 1.23 mmol) was reacted with 3-quinuclidinone hydrochloride and hydrazine hydrate according to the general procedure. Compound **31** was yielded as a yellow solid of 90%. ¹H NMR (600 MHz, DMSO-*d*₆): δ 13.13 (s, 1H), 8.74 (d, *J* = 5.1 Hz, 1H), 8.19–8.18 (m, 1H), 8.05 (dd, *J* = 5.1, 1.6 Hz, 1H), 6.87 (s, 1H), 3.00 (dt, *J* = 12.2, 3.3 Hz, 2H), 2.75 (tt, *J* = 11.8, 3.8 Hz, 1H), 2.57 (td, *J* = 12.1, 2.5 Hz, 2H), 1.88–1.81 (m, 2H), 1.52 (qd, *J* = 12.2, 3.9 Hz, 2H). ¹³C NMR (150 MHz, DMSO-*d*₆): δ 151.47, 151.19, 147.78, 147.56, 146.45, 143.37, 123.14, 122.83, 121.32, 116.36, 116.34, 116.32, 116.30, 101.07, 46.40, 34.18, 33.10. HRMS calcd for (M + H)⁺, 297.1327; found, 297.1325.

4-(3-(Piperidin-4-yl)-1H-pyrazol-5-yl)pyridin-2-amine (32). 2-Aminopyridine-4-carboxaldehyde (150 mg, 1.23 mmol) was reacted with 3-quinuclidinone hydrochloride and hydrazine hydrate according to the general procedure. Compound **32** was yielded as a yellow solid of 36%. ¹H NMR (600 MHz, DMSO-*d*₆): δ 13.48 (s, 1H), 8.17 (s, 2H), 7.98 (d, *J* = 6.7 Hz, 1H), 7.35 (s, 1H), 7.25 (dd, *J* = 6.7, 1.6 Hz, 1H), 6.78 (s, 1H), 3.36 (dt, *J* = 13.1, 3.7 Hz, 2H), 3.05 (dq, *J* = 11.8, 4.0 Hz, 3H), 2.17–2.10 (m, 2H), 1.83–1.74 (m, 2H). ¹³C NMR (150 MHz, DMSO-*d*₆): δ 159.44, 159.23, 159.02, 158.81, 155.07, 136.97, 120.49, 118.51, 116.53, 114.56, 109.54, 106.99, 101.93, 43.18, 30.86, 28.27. HRMS calcd for (M + H)⁺, 244.1557; found, 244.1560.

5-(3-(Piperidin-4-yl)-1H-pyrazol-5-yl)pyridin-2-amine (33). 6-Aminonicotinamide (150 mg, 1.23 mmol) was reacted with 3-

quinuclidinone hydrochloride and hydrazine hydrate according to the general procedure. Compound **33** was yielded as a yellow solid of 51%. ¹H NMR (600 MHz, DMSO-*d*₆): δ 12.42 (s, 1H), 8.30 (d, *J* = 2.4 Hz, 1H), 7.74–7.68 (m, 1H), 6.46 (d, *J* = 8.6 Hz, 1H), 6.29 (s, 1H), 5.98 (s, 2H), 2.98 (dt, *J* = 12.4, 3.4 Hz, 2H), 2.70–2.62 (m, 1H), 2.55 (td, *J* = 12.1, 2.5 Hz, 2H), 1.81 (dd, *J* = 13.3, 3.6 Hz, 2H), 1.49 (qd, *J* = 12.2, 3.9 Hz, 2H). ¹³C NMR (150 MHz, DMSO-*d*₆): δ 159.48, 145.12, 134.47, 108.17, 97.74, 46.58, 34.25, 33.36. HRMS calcd for (M + H)⁺, 244.1557; found, 244.1557.

5-(3-(Piperidin-4-yl)-1H-pyrazol-5-yl)pyrimidin-2-amine (34). 2-Amino-5-pyrimidinecarboxaldehyde (151 mg, 1.23 mmol) was reacted with 3-quinuclidinone hydrochloride and hydrazine hydrate according to the general procedure. Compound **34** was yielded as a yellow solid of 49%. ¹H NMR (600 MHz, DMSO-*d*₆): δ 12.57 (s, 1H), 8.59 (s, 2H), 6.70 (s, 2H), 6.39 (s, 1H), 2.98 (dt, *J* = 12.6, 3.4 Hz, 2H), 2.68 (ddt, *J* = 11.9, 8.2, 3.6 Hz, 1H), 2.55 (td, *J* = 12.0, 2.4 Hz, 2H), 1.84–1.79 (m, 2H), 1.49 (qd, *J* = 12.2, 3.9 Hz, 2H). ¹³C NMR (150 MHz, DMSO-*d*₆): δ 163.25, 155.18, 97.98, 46.52, 34.51, 33.28. HRMS calcd for (M + H)⁺, 245.1509; found, 245.1510.

3-(3-(Piperidin-4-yl)-1H-pyrazol-5-yl)pyridin-2-amine (35). 2-Aminopyridine-3-carboxaldehyde (150 mg, 1.23 mmol) was reacted with 3-quinuclidinone hydrochloride and hydrazine hydrate according to the general procedure. Compound **35** was yielded as a yellow solid of 32%. ¹H NMR (600 MHz, DMSO-*d*₆): δ 12.52 (s, 1H), 7.70 (d, *J* = 3.0 Hz, 1H), 7.56 (t, *J* = 3.9 Hz, 1H), 7.46 (d, *J* = 5.0 Hz, 1H), 6.35 (s, 1H), 2.98 (dt, *J* = 12.2, 3.4 Hz, 2H), 2.68 (tt, *J* = 12.0, 3.8 Hz, 1H), 2.56 (td, *J* = 12.0, 2.5 Hz, 2H), 1.82 (dd, *J* = 13.1, 3.5 Hz, 2H), 1.49 (qd, *J* = 12.2, 3.9 Hz, 2H). ¹³C NMR (150 MHz, DMSO-*d*₆): δ 126.95, 126.29, 120.33, 99.45, 46.55, 34.61, 33.36. HRMS calcd for (M + H)⁺, 244.1557; found, 244.1557.

4-(3-(Piperidin-4-yl)-1H-pyrazol-5-yl)-1H-pyrrolo[2,3-*b*]pyridine (36). 1H-Pyrrolo[2,3-*b*]pyridine-4-carboxaldehyde (179 mg, 1.23 mmol) was reacted with 3-quinuclidinone hydrochloride and hydrazine hydrate according to the general procedure. Compound **36** was yielded as a yellow solid of 55%. ¹H NMR (600 MHz, DMSO-*d*₆): δ 12.93 (s, 1H), 11.64 (s, 1H), 8.21 (d, *J* = 4.9 Hz, 1H), 7.48 (d, *J* = 3.4 Hz, 1H), 7.41 (d, *J* = 5.0 Hz, 1H), 6.97 (d, *J* = 3.5 Hz, 1H), 6.70 (s, 1H), 3.01 (dt, *J* = 12.2, 3.3 Hz, 2H), 2.77 (tt, *J* = 11.9, 3.8 Hz, 1H), 2.59 (td, *J* = 12.1, 2.5 Hz, 2H), 1.91–1.87 (m, 2H), 1.56 (qd, *J* = 12.2, 3.9 Hz, 2H). ¹³C NMR (150 MHz, DMSO-*d*₆): δ 150.00, 143.03, 126.40, 116.25, 112.54, 101.37, 101.19, 46.53, 34.38, 33.21. HRMS calcd for (M + H)⁺, 267.1585; found, 267.1588.

1-Methyl-4-(3-(piperidin-4-yl)-1H-pyrazol-5-yl)-1H-pyrrolo[2,3-*b*]pyridine (37). 1-Methyl-1H-pyrrolo[2,3-*b*]pyridine-4-carboxaldehyde (197 mg, 1.23 mmol) was reacted with 3-quinuclidinone hydrochloride and hydrazine hydrate according to the general procedure. Compound **37** was yielded as a yellow solid of 62%. ¹H NMR (600 MHz, DMSO-*d*₆): δ 12.95 (s, 1H), 8.26 (d, *J* = 5.0 Hz, 1H), 7.53 (d, *J* = 3.4 Hz, 1H), 7.44 (d, *J* = 5.0 Hz, 1H), 6.98 (d, *J* = 3.5 Hz, 1H), 6.71 (s, 1H), 3.84 (s, 3H), 3.02 (dt, *J* = 12.5, 3.4 Hz, 2H), 2.77 (tt, *J* = 11.8, 3.9 Hz, 1H), 2.59 (td, *J* = 12.1, 2.5 Hz, 2H), 1.92–1.86 (m, 2H), 1.57 (qd, *J* = 12.2, 3.9 Hz, 2H). ¹³C NMR (150 MHz, DMSO-*d*₆): δ 148.92, 142.89, 130.36, 116.51, 112.60, 101.27, 100.40, 46.42, 34.27, 33.06, 31.43. HRMS calcd for (M + H)⁺, 282.1713; found, 282.1716.

2-(Dimethylamino)isonicotinaldehyde (38a). A mixture of DMF (8.00 mL, 25.8 mmol) and 10 M KOH (800 mg, 20.0 mmol) was heated at reflux for 5 min. 2-Fluoroisonicotinaldehyde (500 mg, 4.00 mmol) was added, and the resulting mixture was heated for 0.5 h at 95 °C. The mixture was treated with additional 10 M KOH (800 mg, 5.00 mmol) and heated for an additional 0.5 h. The reaction was monitored by TLC and additional portions of 10 M KOH (800 mg, 5.00 mmol) were added in 0.5 h intervals until completion was evident. The reaction mixture was then cooled, diluted with water, and extracted with EA (3×). The organic fractions were combined, dried over anhydrous Na₂SO₄, and concentrated under reduced pressure to give the final product **38a** as a yellow oil. ¹H NMR (600 MHz, chloroform-*d*): δ 9.97 (s, 1H), 8.36 (d, *J* = 5.0 Hz, 1H), 6.93 (dd, *J* = 5.1, 1.2 Hz, 1H), 6.89 (s, 1H), 3.16 (s, 6H).

(Z)-2-((2-(Dimethylamino)pyridin-4-yl)methylene)quinuclidin-3-one (38b). A solution of 3-quinuclidinone hydrochloride (161.63 mg

1.0 mmol), **38a** (150 mg, 1.0 mmol), and NaOH (40 mg, 1.0 mmol) in EtOH (5 mL) was heated at reflux for 5 h. The mixture was cooled, concentrated, diluted with water, and extracted with EA (3×). The organic fractions were combined, dried over anhydrous Na₂SO₄, and concentrated under reduced pressure and purified by flash column chromatography on silica gel, eluting with EtOAc/hexane (1:1, v/v) to give the final product **38b** as a yellow solid (171.3 mg, 67%). ¹H NMR (600 MHz, chloroform-*d*): δ 8.19 (d, *J* = 5.2 Hz, 1H), 7.24 (dd, *J* = 5.3, 1.3 Hz, 1H), 7.03 (d, *J* = 1.4 Hz, 1H), 6.88 (s, 1H), 3.21–3.14 (m, 2H), 3.11 (s, 6H), 3.05–2.99 (m, 2H), 2.66 (p, *J* = 3.0 Hz, 1H), 2.05 (ddd, *J* = 10.4, 6.7, 3.0 Hz, 4H). ¹³C NMR (150 MHz, chloroform-*d*): δ 206.02, 159.82, 148.06, 147.39, 141.83, 123.85, 113.23, 108.41, 47.43, 40.19, 38.16, 25.66. HRMS calcd for (M + H)⁺, 258.1606; found, 258.1601.

N,N-Dimethyl-4-(3-(piperidin-4-yl)-1H-pyrazol-5-yl)pyridin-2-amine (**38**). Compound **38** was got according to the general procedure as a white solid of 65%. ¹H NMR (600 MHz, DMSO-*d*₆): δ 12.80 (s, 1H), 8.06 (d, *J* = 5.2 Hz, 1H), 6.96 (s, 1H), 6.94 (s, 1H), 6.61 (s, 1H), 3.06 (s, 6H), 2.99 (dt, *J* = 12.2, 3.3 Hz, 2H), 2.71 (tt, *J* = 11.9, 3.8 Hz, 1H), 2.56 (td, *J* = 12.1, 2.5 Hz, 2H), 1.86–1.81 (m, 2H), 1.51 (qd, *J* = 12.1, 3.9 Hz, 2H). ¹³C NMR (150 MHz, DMSO-*d*₆): δ 158.39, 153.00, 139.67, 132.54, 99.85, 45.48, 40.51, 33.18, 31.69. HRMS calcd for (M + H)⁺, 272.1875; found, 272.1871.

tert-Butyl (Z)-4-((3-oxoquinolidin-2-ylidene)methyl)pyridin-2-yl)carbamate (**32a-Boc**). A solution of 3-quinolidinone hydrochloride (161.63 mg, 1.0 mmol), *tert*-Butyl (4-formylpyridin-2-yl)carbamate (222.24 mg, 1.0 mmol), and NaOH (40 mg, 1.0 mmol) in EtOH (5 mL) was heated at reflux for 5 h. The mixture was cooled, concentrated, diluted with water, and extracted with EA (3×). The organic fractions were combined, dried over anhydrous Na₂SO₄, and concentrated under reduced pressure and purified by flash column chromatography on silica gel, eluting with EtOAc/hexane (1:1, v/v) to give the final product **32a-Boc** as a yellow solid (171.3 mg, 67%). ¹H NMR (600 MHz, chloroform-*d*): δ 8.28 (d, *J* = 5.3 Hz, 1H), 8.22 (s, 1H), 8.16 (s, 1H), 7.76 (dd, *J* = 5.3, 1.4 Hz, 1H), 6.97 (s, 1H), 3.24–3.17 (m, 2H), 3.03 (ddt, *J* = 14.1, 9.6, 4.5 Hz, 2H), 2.67 (p, *J* = 3.0 Hz, 1H), 2.06 (ddd, *J* = 9.8, 6.2, 2.7 Hz, 4H), 1.56 (s, 9H). ¹³C NMR (150 MHz, chloroform-*d*): δ 205.58, 152.51, 152.32, 148.15, 147.83, 143.22, 122.77, 119.93, 114.54, 47.43, 40.15, 29.71, 28.31, 25.57. HRMS calcd for (M + H)⁺, 330.1818; found, 330.1818.

tert-Butyl (Z)-methyl(4-((3-oxoquinolidin-2-ylidene)methyl)pyridin-2-yl)carbamate (**39a**). **32a-Boc** (100 mg, 0.29 mmol) was dissolved in 5 mL of DCM, and then NaH (23 mg, 0.58 mmol) was added and placed in an ice bath. After 30 min, CH₃I (82 mg, 0.58 mmol) was added to the mixture, and the mixture was stirred for 8 h at room temperature. The mixture was concentrated, diluted with water, and extracted with EA (3×). The organic fractions were combined, dried over anhydrous Na₂SO₄, and concentrated under reduced pressure and purified by flash column chromatography on silica gel, eluting with EtOAc/hexane (1:1, v/v) to give the final product **39a** as a yellow solid (35 mg, 34%). ¹H NMR (600 MHz, chloroform-*d*): δ 8.38 (dd, *J* = 5.1, 1.6 Hz, 1H), 8.00 (s, 1H), 7.70 (d, *J* = 5.1 Hz, 1H), 6.92 (d, *J* = 1.8 Hz, 1H), 3.39 (d, *J* = 1.8 Hz, 3H), 3.21–3.16 (m, 2H), 3.00 (td, *J* = 14.5, 11.6, 6.6 Hz, 2H), 2.66 (q, *J* = 2.9 Hz, 1H), 2.07–2.01 (m, 4H), 1.52 (d, *J* = 2.0 Hz, 9H). ¹³C NMR (150 MHz, chloroform-*d*): δ 205.56, 155.88, 154.33, 148.09, 147.61, 141.96, 122.51, 121.73, 120.99, 81.12, 47.45, 40.09, 34.39, 28.29, 25.54. HRMS calcd for (M + H)⁺, 344.1974; found, 344.1972.

N-Methyl-4-(3-(piperidin-4-yl)-1H-pyrazol-5-yl)pyridin-2-amine (**39**). **39a** was refluxed in 3 mL of 20% hydrazine hydrate for 6 h until solid precipitate formed from the reaction mixture. The solid was collected and reacted with 2 mL of TFA for 1 h and the reaction quenched with ammonium hydroxide. The mixture was filtered and the solid was washed with water and diethyl ether and target compound **39** was got. ¹H NMR (600 MHz, DMSO-*d*₆): δ 12.91–12.64 (m, 1H), 7.96 (d, *J* = 5.3 Hz, 1H), 6.85 (dd, *J* = 5.3, 1.4 Hz, 1H), 6.79 (s, 1H), 6.46 (s, 1H), 6.40 (q, *J* = 4.7 Hz, 1H), 2.99 (dt, *J* = 12.3, 3.4 Hz, 2H), 2.79 (d, *J* = 4.8 Hz, 3H), 2.70 (tq, *J* = 13.1, 5.3, 4.5 Hz, 1H), 2.56 (td, *J* = 12.0, 2.5 Hz, 2H), 1.86–1.79 (m, 2H), 1.50 (qd, *J* = 12.2, 3.9 Hz, 2H). ¹³C NMR (150 MHz, DMSO-*d*₆): δ 160.51, 148.46, 108.84, 103.03,

99.66, 46.49, 33.19, 28.60. HRMS calcd for (M + H)⁺, 258.1718; found, 258.1712.

tert-Butyl (Z)-ethyl(4-((3-oxoquinolidin-2-ylidene)methyl)pyridin-2-yl)carbamate (**40a**). **32a-Boc** (100 mg, 0.29 mmol) was dissolved in 5 mL of DCM and then NaH (23 mg, 0.58 mmol) was added and placed in an ice bath. After 30 min, iodoethane (90.4 mg, 0.58 mmol) was added to the mixture, and the mixture was stirred for 8 h at room temperature. The mixture was concentrated, diluted with water, and extracted with EA (3×). The organic fractions were combined, dried over anhydrous Na₂SO₄, and concentrated under reduced pressure and purified by flash column chromatography on silica gel, eluting with EtOAc/hexane (1:1, v/v) to give the final product **40a** as a yellow solid (35 mg, 34%). ¹H NMR (600 MHz, chloroform-*d*): δ 8.40 (d, *J* = 5.2 Hz, 1H), 7.94 (s, 1H), 7.74 (d, *J* = 5.3 Hz, 1H), 6.93 (s, 1H), 3.97 (q, *J* = 7.2, 6.8 Hz, 2H), 3.24–2.96 (m, 4H), 2.68 (s, 1H), 2.06 (m, 4H), 1.53 (s, 9H), 1.28 (t, 3H). ¹³C NMR (150 MHz, chloroform-*d*): δ 205.61, 155.29, 154.04, 148.05, 147.84, 141.98, 122.57, 122.35, 121.11, 47.44, 42.20, 40.12, 28.32, 25.57, 14.18. HRMS calcd for (M + H)⁺, 358.2131; found, 358.2130.

N-Ethyl-4-(3-(piperidin-4-yl)-1H-pyrazol-5-yl)pyridin-2-amine (**40**). Compound **40** was got according to the procedure as compound **39**. ¹H NMR (600 MHz, DMSO-*d*₆): δ 13.44 (s, 1H), 9.00–8.93 (m, 1H), 8.76–8.66 (m, 1H), 7.96 (d, *J* = 6.6 Hz, 1H), 7.33 (s, 1H), 7.22 (d, *J* = 6.6 Hz, 1H), 6.82 (s, 1H), 3.37 (t, *J* = 11.2 Hz, 4H), 3.09–3.00 (m, 3H), 2.15 (dd, *J* = 14.2, 3.7 Hz, 2H), 1.80 (qd, *J* = 12.6, 3.9 Hz, 2H), 1.23 (t, *J* = 7.2 Hz, 3H). ¹³C NMR (150 MHz, DMSO-*d*₆): δ 159.20, 158.99, 158.78, 158.57, 153.57, 120.50, 118.52, 116.54, 114.55, 109.19, 102.02, 43.19, 37.06, 28.30, 14.11. HRMS calcd for (M + H)⁺, 272.1870; found, 272.1872.

4-(3-(1-Methylpiperidin-4-yl)-1H-pyrazol-5-yl)pyridine (**41**). Tri-fluoroacetic acid (4 mL, 106 mmol) was added dropwise over 1 h to a stirred suspension of **1** (200 mg, 1.6 mmol), sodium borohydride (304 mg, 8.0 mmol), and paraformaldehyde (324 μL, 16 mmol) in dry THF (10 mL) under nitrogen. After stirring for 20 h, the mixture was poured into ice-cold 10% aqueous NaOH (20 mL) and extracted with DCM (3 × 10 mL). The combined organic extracts were washed with brine, dried, evaporated, and purified by flash column chromatography on silica gel, eluting with DCM/MeOH (20:1, v/v) to give the final product **41** as a white solid (20 mg, 10%). ¹H NMR (600 MHz, DMSO-*d*₆): δ 12.99 (s, 1H), 8.57 (d, *J* = 4.8 Hz, 2H), 7.75–7.70 (m, 2H), 6.75–6.67 (m, 1H), 3.42–3.33 (m, 2H), 3.10–2.99 (m, 2H), 2.78–2.70 (m, 1H), 2.44–2.37 (m, 3H), 2.04–1.97 (m, 2H), 1.82–1.71 (m, 2H). ¹³C NMR (150 MHz, DMSO-*d*₆): δ 150.55, 141.45, 119.85, 100.43, 54.68, 45.33, 31.98, 30.77. HRMS calcd for (M + H)⁺, 243.1610; found, 243.1614.

Molecular Docking. Molecular docking was performed using MOE with the AMBER10: EHT force field. The crystal structure of MNK2 was selected, downloaded from the Protein Data Bank (PDB, <http://www.rcsb.org>), and was used for docking. The induced fit docking approach was applied with consideration for the side chain flexibility of residues at the binding site. The ligand binding site was defined using the bound ligands in the crystal structures. The best scored conformation with minimum binding energy from the 30 docking conformations of the ligands was selected for analysis.

MD Simulation. The AMBER16 package and ff14SB force field were used to perform MD simulations to optimize the complex. The complex was solvated in a 10 Å TIP3P water box. The electrical properties were neutralized using Cl⁻ and MD simulation was run using the Bash command. The system was optimized by the 2000-step steepest descent and the 3000-step conjugate gradient. After the first energy optimization was completed, the unconstrained optimization continued, and was followed by MD simulations. MD simulations include both warming and equilibration processes. First, the systems were gradually heated from 50 to 300 K with the solute restrained to their position using 5 kcal mol⁻¹·Å⁻² within 100 ps. For the equilibrium process, the solute binding force was gradually reduced from 5 to 0 kcal mol⁻¹·Å⁻² within 100 ps. Then, 100 ns simulations were conducted at a constant temperature of 300 K and with the pressure at 1 atm. The SHAKE algorithm was used for all the hydrogen bonds involved, and a time step of 2 fs was used. After the MD simulation, the MD trajectories

were analyzed using VMD (<http://www.ks.uiuc.edu/>), and root-mean-square deviation (rmsd) values were calculated.

Kinase-Inhibition Assays. Compound D25 was tested at 1 μM against a panel of 70 kinases through the commercially available service provided by ICE Bioscience (Beijing, China).

Kinase Activity Assays. MNK1 and MNK2 kinase inhibition assays were done using LANCE Ultra Kinase Assays from PerkinElmer. Compound staurosporine was used as a positive control. Briefly, 1.00 ng of MNK1 or 0.05 ng of MNK2 was incubated with different concentrations (10,000, 1000, 100, 10, 1 nM) of test compounds in a 10 μL reaction mixture [MNK1:12.5 nM CREB, 450 μM ATP, 2 mM DTT, 1 \times buffer; MNK2:12.5 nM CREB, 100 μM ATP, 2 mM DTT, 1 \times buffer] for 60 min at 25 $^{\circ}\text{C}$. The mixture of 5 μL of EDTA/detection buffer and 5 μL of Eu-CREB/detection buffer was added to terminate the reaction for 60 min. The ratio between the homogeneous time-resolved fluorescence signals of 615 and 665 nm was recorded, and IC_{50} values were calculated from the inhibition curves.

Pharmacokinetic Profile Analysis. The pharmacokinetic analysis of D25 was conducted in male SD rats (Pengyue, Jinan). The HCl salt of compound D25 was dissolved in saline. The compound D25 was administered to SD rats intravenously (iv) via the tail vein at 5 mg/kg ($n = 3$) and via intragastric administration at 20 mg/kg ($n = 3$). The blood samples were taken at 0.033, 0.083, 0.25, 0.5, 1, 2, 4, 6, 8, 12, 24, and 48 h time points of the route of i.v. and at 0.083, 0.25, 0.5, 1, 2, 4, 6, 8, 12, 24, and 48 h time points of the route of p.o. Samples were placed in tubes containing K2-EDTA and stored on ice until centrifugation. The blood samples were centrifuged at 12,000 rpm for 5 min at 4 $^{\circ}\text{C}$ for 1 h, and plasma was collected and stored frozen at approximately -20°C . An aliquot of 50 μL of the plasma sample was mixed with 200 μL of methanol, and the mixture was vortexed for 5 min and the upper layer was used for compound analysis. The analytical results were confirmed using quality control samples for intra-assay variation. A standard set of parameters including area under the curve [AUC_{0-t} (last) and $\text{AUC}_{0-\infty}$], elimination half-life ($T_{1/2}$), maximum plasma concentration (C_{max}), and time to reach the maximum plasma concentration (T_{max}) were calculated using noncompartmental analysis modules in the FDA-certified pharmacokinetic program Phoenix WinNonlin 7.0 (Pharsight, USA).

Cell Culture. Mouse monocyte macrophage leukemia cells (RAW264.7) and MV-4-11 cells were purchased from Procell Life Science&Technology Co., Ltd. The RAW264.7 cells were cultured in DMEM supplemented with 10% fetal bovine serum (FBS) and 1% penicillin-streptomycin. MV-4-11 cells were cultured in Roswell Park Memorial Institute-1640 (RPMI-1640) media (2 g/L glucose) containing 10% FBS and 1% penicillin-streptomycin.

Cell Viability Assay. RAW264.7 cell viability was assessed using the brominated 3-(4,5-dimethylthiazol-2-yl)-2,5-diphenyltetrazolium (MTT) assay. Initially, 5×10^3 cells/well were seeded in 96-well plates, and these cells were treated with compounds and DEX at indicated concentrations for 24 h. Following treatment, 20 μL of MTT (5 mg/mL) was added to each well at the corresponding time points. After an incubation period of 4 h, 150 μL of dimethyl sulfoxide (DMSO) was added to each well and incubated at room temperature for 30 min to solubilize the formazan crystals. Eventually, the optical density (OD) was measured using a microplate reader (PE, envision, US) at an absorbance of 490 nm.

Cell viability in MV-4-11 was evaluated using the Cell Counting Kit-8 (CCK-8, GLP BIO Technology). Cells were seeded at a density of 5×10^3 cells per well in 96-well plates and were exposed to the test compounds at a concentration of 20 μM for 48 h. Following the incubation with compounds, 20 μL of the CCK-8 reagent was dispensed into each well at the appropriate time points. A 4 h incubation ensued, post which the OD was recorded using the same microplate reader (PE EnVision, USA) at an absorbance wavelength of 450 nm.

Western Blot Analysis. Protein extraction from RAW264.7 cells and spleen tissue was carried out using RIPA buffer supplemented with phenylmethylsulfonyl fluoride (PMSF; Beyotime) at a 100:1 ratio. Protein concentrations were quantified with a BCA protein detection kit. Equal amounts of protein were subjected to SDS-PAGE and

transferred onto polyvinylidene difluoride (PVDF) membranes (preactivated with methanol 5 min). Membranes were blocked with blocking buffer (Beyotime) for 0.5–1 h. Overnight incubation at 4 $^{\circ}\text{C}$ with primary antibody was followed by a 2 h incubation with the appropriate HRP-conjugated secondary antibodies at room temperature. Enhanced chemiluminescence (super ECL plus, Beyotime) was used to visualize protein bands, which were imaged on a Chemiluminescence Apparatus (Bio-Rad, US). Band intensity was quantified using ImageJ software (National Institutes of Health, Bethesda, MD, USA). Primary antibodies: COX-2 (1:2000), i-NOS (1:2000), TNF- α (1:2000), IL-6 (1:2000) (all from Affinity); eIF4E (1:5000) and p-eIF4E (Ser209) (1:5000) (both from Abcam); and GAPDH (1:2000) and β -actin (1:2000) (both from Proteintech, Shanghai, China). Secondary antibody: sheep antirabbit/mouse IgG H&L secondary antibody (horseradish peroxidase); goat antirabbit/mouse IgG H&L secondary antibody (horseradish peroxidase) (1:2000; ORIGENE, Beijing, China).

Establishing the LPS-Induced Sepsis In Vivo Model and Treatment. Balb/c male mice (weight: 18–21 g) were utilized to establish LPS-induced spleen injury in acute sepsis model. Forty mice were randomly divided into five groups: control (Con), sepsis (LPS), two D25-pretreated groups (10, 20 mg/kg), and a DEX (2.5 mg/kg) pretreated group. The control and LPS groups were given equal amounts of 0.5% CMC-Na by intragastric administration for 14 days. D25 was mixed in 0.5% CMC-Na and administered by gavage at 10 and 20 mg/kg for 14 days, respectively. After 14 days, LPS, D25, and DEX groups received an intraperitoneal injection of 10 mg/kg LPS to induce sepsis and associated spleen injury. Six hours post-LPS injection, mice were euthanized, and samples of blood and spleen were collected and stored at -80°C for subsequent analysis.

Biochemical Analysis. Blood serum separated by centrifugation was analyzed for IL-6, IL-1 β , and TNF- α using ELISA kits from Quanzhou Ruixin Biotechnology Co., Ltd. Antioxidant and oxidative stress markers SOD, GSH, and MDA were quantified using kits from the same company. Kidney function was assessed by measuring BUN and creatinine using kits from Nanjing Jiancheng Bioengineering Institute. Liver injury markers ALT, AST, and LDH were evaluated with an automated analyzer from Rayto Life and Analytical Sciences Co., Ltd.

Histopathological Examination. Fresh spleen tissues were fixed with 4% paraformaldehyde (Servicebio, Wuhan, China), embedded in paraffin, and sectioned at 5 μm for hematoxylin and eosin staining (H&E). Sections were examined under an Olympus IX73 Fluorescence Microscope. For macrophage immunohistochemistry, spleen sections were deparaffinized with xylene, rehydrated with different concentrations of alcohol (100, 95, 85, 75%), and washed with water. They underwent antigen retrieval with Tris-EDTA buffer (pH 8.0). Endogenous catalase was then inactivated using 3% H_2O_2 . Post blocking with 5% BSA, slides were incubated with the F4/80 antibody (Servicebio) overnight at 4 $^{\circ}\text{C}$, followed by HRP-conjugated secondary antibody (ZSGB-BIO) and DAB staining. After counterstaining with hematoxylin and dehydration, sections were visualized under the same microscope.

Flow Cytometry Assessment of ROS. The effects of D25 and DEX on ROS production in LPS-stimulated RAW264.7 macrophages were investigated using the DCF-DA method.³⁸ Cells at 80% confluency were pretreated with D25, challenged with LPS (1 $\mu\text{g}/\text{mL}$) for 1 h, and stained with DCF-DA. ROS levels were analyzed by flow cytometry (Cytek Aurora).

Immunofluorescence Assay. RAW 264.7 macrophages (5×10^3 cells/chamber) were cultured in eight-chamber culture slides and incubated for 24 h before D25 treatment. The cells were pretreated with D25 or DEX for 1 h and stimulated with LPS (1 $\mu\text{g}/\text{mL}$) for 1 h. The medium was washed away with PBS, and the cells were fixed with 4% paraformaldehyde for 15 min. Cells were blocked with a blocking solution (PBS containing 5% BSA and 0.3% Triton X-100) for 1 h and then incubated overnight at 4 $^{\circ}\text{C}$ with the p-eIF4E antibody (1:200, Abcam). The next day, cells were plated at room temperature for 30 min and treated with Goat Anti Mouse IgG (H&L)-Alexa Fluor 488 (Immunoway, USA) for 1 h. The nuclei were stained with DAPI

staining solution (Beijing Solarbio Technology Co., Ltd.). Images were collected with a laser confocal microscope (Olympus, FV3000, Japan).

Measurement of NO Production. The Griess assay was used to quantify NO production in LPS-stimulated RAW264.7 macrophages. Cells were seeded in 96-well plates, pretreated with D25 or DEX, and then exposed to LPS (50 ng/mL). Griess reagent was added, and absorbance was measured at 540 nm using a PE EnVision microplate reader.

Statistical Analysis. All in vitro experiments were performed in triplicate, and quantitative data are shown as the average of all biological replicates. All statistical analyses were performed using GraphPad Prism 7 (GraphPad Software). For simple comparisons, an unpaired two-tailed Student's *t*-test was used. In all cases, *n* refers to the number of repetitions.

■ ASSOCIATED CONTENT

SI Supporting Information

The Supporting Information is available free of charge at <https://pubs.acs.org/doi/10.1021/acs.jmedchem.3c02441>.

Kinase profiling; PK parameters of compound D25; and ¹H, ¹³C, and HPLC spectra of all compounds (PDF)

Molecular formula strings (CSV)

■ AUTHOR INFORMATION

Corresponding Authors

Yue-Wei Guo – Shandong Laboratory of Yantai Drug Discovery, Bohai Rim Advanced Research Institute for Drug Discovery, Yantai 264117, China; School of Medicine, Shanghai University, Shanghai 200444, China; orcid.org/0000-0003-0413-2070; Email: ywguo@sim.ac.cn

Mingzhi Su – Shandong Laboratory of Yantai Drug Discovery, Bohai Rim Advanced Research Institute for Drug Discovery, Yantai 264117, China; Email: mzsu@baridd.ac.cn

Xin Jin – Shandong Laboratory of Yantai Drug Discovery, Bohai Rim Advanced Research Institute for Drug Discovery, Yantai 264117, China; Email: xjin@baridd.ac.cn

Authors

Qiang Li – Shandong Laboratory of Yantai Drug Discovery, Bohai Rim Advanced Research Institute for Drug Discovery, Yantai 264117, China; Shandong First Medical University & Shandong Academy of Medical Sciences, Jinan 250117, China

Linmao Ke – Shandong Laboratory of Yantai Drug Discovery, Bohai Rim Advanced Research Institute for Drug Discovery, Yantai 264117, China; Guangdong Provincial Key Laboratory of Research and Development of Natural Drugs, and School of Pharmacy, Guangdong Medical University, Zhanjiang 524023, China

Dandan Yu – Shandong Laboratory of Yantai Drug Discovery, Bohai Rim Advanced Research Institute for Drug Discovery, Yantai 264117, China; Guangdong Provincial Key Laboratory of Research and Development of Natural Drugs, and School of Pharmacy, Guangdong Medical University, Zhanjiang 524023, China

Han Xu – Shandong Laboratory of Yantai Drug Discovery, Bohai Rim Advanced Research Institute for Drug Discovery, Yantai 264117, China; School of Pharmacy, Yantai University, Yantai 264005, China

Zixuan Zhang – School of Medicine and Pharmacy, Ocean University of China, Qingdao 266003, China

Rilei Yu – School of Medicine and Pharmacy, Ocean University of China, Qingdao 266003, China; orcid.org/0000-0001-6625-2014

Tao Jiang – School of Medicine and Pharmacy, Ocean University of China, Qingdao 266003, China; orcid.org/0000-0002-6590-5041

Complete contact information is available at:

<https://pubs.acs.org/10.1021/acs.jmedchem.3c02441>

Author Contributions

XJ performed the experiments, analyzed the data, and wrote the paper. QL, LMK, DDY, and HX performed some of the experiments. ZXZ, RLY, and TJ performed the MD stimulation. MZS, XJ, and YWG designed and supervised the research.

Notes

The authors declare no competing financial interest.

■ ACKNOWLEDGMENTS

We are grateful to the National Key Research and Development Program of China (No. 2022YFC2804100), the National Natural Science Foundation of China (Grant no. 81991521), the Natural Science Foundation of Shandong Province (ZR2022QH139), and the Shandong Laboratory Program (SYS202205).

■ ABBREVIATIONS

AST, alanine aminotransferase; ALT, aspartate aminotransferase; AML, acute myeloid leukemia; BUN, urea nitrogen; CRE, creatinine; COX-2, cyclooxygenase-2; DEX, dexamethasone; eIF4E, eukaryotic initiation factor 4E; GSH, glutathione; IL-6, interleukin-6; IL-1 β , interleukin-1 β ; iNOS, inducible NO synthase; LDH, lactate dehydrogenase; LPS, lipopolysaccharide; MDA, malondialdehyde; MNKS, mitogen-activated protein kinase-interacting protein kinases; NSCLC, nonsmall cell lung cancer; NO, nitric oxide; PGs, prostaglandins; ROS, reactive oxygen species; TME, tumor microenvironment; TNF α , tumor necrosis factor α ; TLR, Toll-like receptor

■ REFERENCES

- (1) Konicek, B. W.; Dumstorf, C. A.; Graff, J. R. Targeting the eIF4F translation initiation complex for cancer therapy. *Cell Cycle* **2008**, *7*, 2466–2471.
- (2) Diab, S.; Kumarasiri, M.; Yu, M.; Teo, T.; Proud, C.; Milne, R.; Wang, S. MAP kinase-interacting kinases-emerging targets against cancer. *Chem. Biol.* **2014**, *21*, 441–452.
- (3) Jin, X.; Yu, R.; Wang, X.; Proud, C. G.; Jiang, T. Progress in developing MNK inhibitors. *Eur. J. Med. Chem.* **2021**, *219*, 113420.
- (4) Xu, W.; Kannan, S.; Verma, C. S.; Nacro, K. Update on the development of MNK inhibitors as therapeutic agents. *J. Med. Chem.* **2022**, *65*, 983–1007.
- (5) Hay, N. Mnk earmarks eIF4E for cancer therapy. *Proc. Natl. Acad. Sci. U.S.A.* **2010**, *107*, 13975–13976.
- (6) Robichaud, N.; del Rincon, S. V.; Huor, B.; Alain, T.; Petruccioli, L. A.; Hearnden, J.; Goncalves, C.; Grotegut, S.; Spruck, C. H.; Furic, L.; Larsson, O.; Muller, W. J.; Miller, W. H.; Sonenberg, N. Phosphorylation of eIF4E promotes EMT and metastasis via translational control of SNAIL and MMP-3. *Oncogene* **2015**, *34*, 2032–2042.
- (7) Robichaud, N.; Hsu, B. E.; Istomine, R.; Alvarez, F.; Blagih, J.; Ma, E. H.; Morales, S. V.; Dai, D. L.; Li, G.; Souleimanova, M.; Guo, Q.; Del Rincon, S. V.; Miller, W. H., Jr.; Ramón y Cajal, S.; Park, M.; Jones, R. G.; Piccirillo, C. A.; Siegel, P. M.; Sonenberg, N. Translational control in the tumor microenvironment promotes lung metastasis: Phosphorylation of eIF4E in neutrophils. *Proc. Natl. Acad. Sci. U.S.A.* **2018**, *115*, No. E2202.
- (8) Ueda, T.; Sasaki, M.; Elia, A. J.; Chio, I. I.; Hamada, K.; Fukunaga, R.; Mak, T. W. Combined deficiency for MAP kinase-interacting kinase

- 1 and 2 (Mnk1 and Mnk2) delays tumor development. *Proc. Natl. Acad. Sci. U.S.A.* **2010**, *107*, 13984–13990.
- (9) Furic, L.; Rong, L.; Larsson, O.; Koumakpayi, I. H.; Yoshida, K.; Brueschke, A.; Petroulakis, E.; Robichaud, N.; Pollak, M.; Gaboury, L. A.; Pandolfi, P. P.; Saad, F.; Sonenberg, N. eIF4E phosphorylation promotes tumorigenesis and is associated with prostate cancer progression. *Proc. Natl. Acad. Sci. U.S.A.* **2010**, *107*, 14134–14139.
- (10) Ueda, T.; Watanabe-Fukunaga, R.; Fukuyama, H.; Nagata, S.; Fukunaga, R. Mnk2 and Mnk1 are essential for constitutive and inducible phosphorylation of eukaryotic initiation factor 4E but not for cell growth or development. *Mol. Cell. Biol.* **2004**, *24*, 6539–6549.
- (11) Hwang, J. S.; Kim, K. H.; Park, J.; Kim, S. M.; Cho, H.; Lee, Y.; Han, I. O. Glucosamine improves survival in a mouse model of sepsis and attenuates sepsis-induced lung injury and inflammation. *J. Biol. Chem.* **2019**, *294*, 608–622.
- (12) Zhao, Y.; Yang, Y.; Liu, M.; Qin, X.; Yu, X.; Zhao, H.; Li, X.; Li, W. COX-2 is required to mediate crosstalk of ROS-dependent activation of MAPK/NF-kappaB signaling with pro-inflammatory response and defense-related NO enhancement during challenge of macrophage-like cell line with *Giardia duodenalis*. *PLoS Neglected Trop. Dis.* **2022**, *16*, No. e0010402.
- (13) Fink, M. P.; Warren, H. S. Strategies to improve drug development for sepsis. *Nat. Rev. Drug Discovery* **2014**, *13*, 741–758.
- (14) Jeevakumar, V.; Al Sardar, A. K.; Mohamed, F.; Smithhart, C. M.; Price, T.; Dussor, G. IL-6 induced upregulation of T-type Ca(2+) currents and sensitization of DRG nociceptors is attenuated by MNK inhibition. *J. Neurophysiol.* **2020**, *124*, 274–283.
- (15) Moy, J. K.; Khoutorsky, A.; Asiedu, M. N.; Black, B. J.; Kuhn, J. L.; Barragan-Iglesias, P.; Megat, S.; Burton, M. D.; Burgos-Vega, C. C.; Melemedjian, O. K.; Boitano, S.; Vagner, J.; Gkogkas, C. G.; Pancrazio, J. J.; Mogil, J. S.; Dussor, G.; Sonenberg, N.; Price, T. J. The MNK-eIF4E Signaling Axis Contributes to Injury-Induced Nociceptive Plasticity and the Development of Chronic Pain. *J. Neurosci.* **2017**, *37*, 7481–7499.
- (16) Andersson, K.; Sundler, R. Posttranscriptional regulation of TNF α expression via eukaryotic initiation factor 4E (eIF4E) phosphorylation in mouse macrophages. *Cytokine* **2006**, *33*, 52–57.
- (17) Buxade, M.; Parra, J. L.; Rousseau, S.; Shpiro, N.; Marquez, R.; Morrice, N.; Bain, J.; Espel, E.; Proud, C. G. The Mnk2s Are Novel Components in the Control of TNF α Biosynthesis and Phosphorylate and Regulate hnRNP A1. *Immunity* **2005**, *23*, 177–189.
- (18) Cherla, R. P.; Lee, S. Y.; Mees, P. L.; Tesh, V. L. Shiga toxin 1-induced cytokine production is mediated by MAP kinase pathways and translation initiation factor eIF4E in the macrophage-like THP-1 cell line. *J. Leukocyte Biol.* **2005**, *79*, 397–407.
- (19) Rowlett, R. M.; Chrestensen, C. A.; Nyce, M.; Harp, M. G.; Pelo, J. W.; Cominelli, F.; Ernst, P. B.; Pizarro, T. T.; Sturgill, T. W.; Worthington, M. T. MNK kinases regulate multiple TLR pathways and innate proinflammatory cytokines in macrophages. *Am. J. Physiol.: Gastrointest. Liver Physiol.* **2008**, *294*, G452–G459.
- (20) Bao, Y.; Wu, X.; Chen, J.; Hu, X.; Zeng, F.; Cheng, J.; Jin, H.; Lin, X.; Chen, L. F. Brd4 modulates the innate immune response through Mnk2–eIF4E pathway-dependent translational control of I κ B α . *Proc. Natl. Acad. Sci. U.S.A.* **2017**, *114*, No. E3993.
- (21) Gao, J.; Teng, L.; Yang, S.; Huang, S.; Li, L.; Zhou, L.; Liu, G.; Tang, H. MNK as a potential pharmacological target for suppressing LPS-induced acute lung injury in mice. *Biochem. Pharmacol.* **2021**, *186*, 114499.
- (22) Kjellerup, R. B.; Kragballe, K.; Iversen, L.; Johansen, C. Pro-inflammatory cytokine release in keratinocytes is mediated through the MAPK signal-integrating kinases. *Exp. Dermatol.* **2008**, *17*, 498–504.
- (23) Bartish, M.; Tong, D.; Pan, Y.; Wallerius, M.; Liu, H.; Ristau, J.; de Souza Ferreira, S.; Wallmann, T.; van Hoef, V.; Masvidal, L.; Kerzel, T.; Joly, A. L.; Goncalves, C.; Preston, S. E. J.; Ebrahimian, T.; Seitz, C.; Bergh, J.; Pietras, K.; Lehoux, S.; Naldini, L.; Andersson, J.; Squadrito, M. L.; Del Rincon, S. V.; Larsson, O.; Rolny, C. MNK2 governs the macrophage antiinflammatory phenotype. *Proc. Natl. Acad. Sci. U.S.A.* **2020**, *117*, 27556–27565.
- (24) Jin, X.; Qiu, T.; Xie, J.; Wei, X.; Wang, X.; Yu, R.; Proud, C.; Jiang, T. Using Imidazo[2,1-b][1,3,4]thiadiazol Skeleton to Design and Synthesize Novel MNK Inhibitors. *ACS Med. Chem. Lett.* **2023**, *14*, 83–91.
- (25) Jin, X.; Merrett, J.; Tong, S.; Flower, B.; Xie, J.; Yu, R.; Tian, S.; Gao, L.; Zhao, J.; Wang, X.; Jiang, T.; Proud, C. G. Design, synthesis and activity of Mnk1 and Mnk2 selective inhibitors containing thieno[2,3-d]pyrimidine scaffold. *Eur. J. Med. Chem.* **2019**, *162*, 735–751.
- (26) Jin, X.; Li, M.; Qiu, T.; Yu, R.; Jiang, T. Design, Synthesis and Evaluation of Novel Phorbazole C Derivatives as MNK Inhibitors through Virtual High-Throughput Screening. *Mar. Drugs* **2022**, *20*, 429.
- (27) Santag, S.; Siegel, F.; Wengner, A. M.; Lange, C.; Bomer, U.; Eis, K.; Puhler, F.; Lienau, P.; Bergemann, L.; Michels, M.; von Nussbaum, F.; Mumberg, D.; Petersen, K. BAY 1143269, a novel MNK1 inhibitor, targets oncogenic protein expression and shows potent anti-tumor activity. *Cancer Lett.* **2017**, *390*, 21–29.
- (28) Reich, S. H.; Sprengeler, P. A.; Chiang, G. G.; Appleman, J. R.; Chen, J.; Clarine, J.; Eam, B.; Ernst, J. T.; Han, Q.; Goel, V. K.; Han, E. Z. R.; Huang, V.; Hung, I. N. J.; Jemison, A.; Jessen, K. A.; Molter, J.; Murphy, D.; Neal, M.; Parker, G. S.; Shaghafi, M.; Sperry, S.; Staunton, J.; Stumpf, C. R.; Thompson, P. A.; Tran, C.; Webber, S. E.; Wegerski, C. J.; Zheng, H.; Webster, K. R. Structure-based Design of Pyridone-Aminal eFT508 Targeting Dysregulated Translation by Selective Mitogen-activated Protein Kinase Interacting Kinases 1 and 2 (MNK1/2) Inhibition. *J. Med. Chem.* **2018**, *61*, 3516–3540.
- (29) Yang, H.; Chennamaneni, L. R.; Ho, M. W. T.; Ang, S. H.; Tan, E. S. W.; Jeyaraj, D. A.; Yeap, Y. S.; Liu, B.; Ong, E. H.; Joy, J. K.; Wee, J. L. K.; Kwek, P.; Retna, P.; Dinie, N.; Nguyen, T. T. H.; Tai, S. J.; Manoharan, V.; Pendharker, V.; Low, C. B.; Chew, Y. S.; Vuddagiri, S.; Sangthongpitag, K.; Choong, M. L.; Lee, M. A.; Kannan, S.; Verma, C. S.; Poulsen, A.; Lim, S.; Chuah, C.; Ong, T. S.; Hill, J.; Matter, A.; Nacro, K. Optimization of Selective Mitogen-Activated Protein Kinase Interacting Kinases 1 and 2 Inhibitors for the Treatment of Blast Crisis Leukemia. *J. Med. Chem.* **2018**, *61*, 4348–4369.
- (30) Rowley, M.; Collins, I.; Broughton, H. B.; Davey, W. B.; Baker, R.; Emms, F.; Marwood, R.; Patel, S.; Patel, S.; Ragan, C. I.; Freedman, S. B.; Ball, R.; Leeson, P. D. 4-Heterocyclylpiperidines as selective high-affinity ligands at the human dopamine D4 receptor. *J. Med. Chem.* **1997**, *40*, 2374–2385.
- (31) Jauch, R.; Cho, M. K.; Jakel, S.; Netter, C.; Schreiter, K.; Aicher, B.; Zweckstetter, M.; Jackle, H.; Wahl, M. C. Mitogen-activated protein kinases interacting kinases are autoinhibited by a reprogrammed activation segment. *EMBO J.* **2006**, *25*, 4020–4032.
- (32) Hou, J.; Teo, T.; Sykes, M. J.; Wang, S. Insights into the Importance of DFD-Motif and Insertion I1 in Stabilizing the DFD-Out Conformation of Mnk2 Kinase. *ACS Med. Chem. Lett.* **2013**, *4*, 736–741.
- (33) Kannan, S.; Pradhan, M. R.; Cherian, J.; Joseph, T. L.; Poh, Z. Y.; Hai Yan, Y.; Melvyn, H.; Boping, L.; Jeffrey, H.; Nacro, K.; Verma, C. S. Small Molecules Targeting the Inactive Form of the Mnk1/2 Kinases. *ACS Omega* **2017**, *2*, 7881–7891.
- (34) Oyarzabal, J.; Zarich, N.; Albarran, M. I.; Palacios, I.; Urbano-Cuadrado, M.; Mateos, G.; Reymundo, I.; Rabal, O.; Salgado, A.; Corriero, A.; Fominaya, J.; Pastor, J.; Bischoff, J. R. Discovery of mitogen-activated protein kinase-interacting kinase 1 inhibitors by a comprehensive fragment-oriented virtual screening approach. *J. Med. Chem.* **2010**, *53*, 6618–6628.
- (35) Kieler, M.; Hofmann, M.; Schabbauer, G. More than just protein building blocks: how amino acids and related metabolic pathways fuel macrophage polarization. *FEBS J.* **2021**, *288*, 3694–3714.
- (36) Zhang, W.; Chen, H.; Xu, Z.; Zhang, X.; Tan, X.; He, N.; Shen, J.; Dong, J. Liensinine pretreatment reduces inflammation, oxidative stress, apoptosis, and autophagy to alleviate sepsis acute kidney injury. *Int. Immunopharmacol.* **2023**, *122*, 110563.
- (37) Khan, A. M.; Khan, A. U.; Ali, H.; Islam, S. U.; Seo, E. K.; Khan, S. Continentalic acid exhibited nephroprotective activity against the LPS and E. coli-induced kidney injury through inhibition of the oxidative stress and inflammation. *Int. Immunopharmacol.* **2020**, *80*, 106209.

(38) Yang, L.; Liu, G.; Li, X.; Xia, Z.; Wang, Y.; Lin, W.; Zhang, W.; Zhang, W.; Li, X. Small GTPase RAB6 deficiency promotes alveolar progenitor cell renewal and attenuates PM2.5-induced lung injury and fibrosis. *Cell Death Dis.* **2020**, *11*, 827.